FAULT DIAGNOSIS OF A LAUNCH VEHICLE ACTUATION SYSTEM USING WAVELET NEURAL NETWORK

A PROJECT REPORT

submitted by

ANJANA VIJAYAN
(Reg. No. TKM20EEII06)

to

the APJ Abdul Kalam Technological University
in partial fulfillment of the requirements for the award of the Degree

of

Master of Technology
in
Electrical and Electronics Engineering

with specialisation in

Industrial Instrumentation and Control

Department of Electrical and Electronics Engineering
TKM College of Engineering
Kollam - 691 005
KERALA

JULY 2022

DECLARATION

I undersigned hereby declare that the project report entitled "**Fault Diagnosis of a Launch Vehicle Actuation System using Wavelet Neural Network**", submitted for partial fulfillment of the requirements for the award of degree of Master of Technology in Electrical and Electronics Engineering with specialisation in Industrial Instrumentation and Control, of the APJ Abdul Kalam Technological University, Kerala is a bonafide work done by me under supervision of *Mr. Baby Sebastian*, Scientist, DH, SDCD, CESG, VSSC Thiruvananthapuram, and *Prof. Asha Ravindranath*, Associate Professor, Department of EEE, TKM College of Engineering. This submission represents my ideas in my own words and where ideas or words of others have been included, I have adequately and accurately cited and referenced the original sources. I also declare that I have adhered to ethics of academic honesty and integrity and have not misrepresented or fabricated any data or idea or fact or source in my submission. I understand that any violation of the above will be a cause for disciplinary action by the institute and/or the University and can also evoke penal action from the sources which have thus not been properly cited or from whom proper permission has not been obtained. This report has not been previously formed the basis for the award of any degree, diploma or similar title of any other University.

Kollam
July 01, 2022

ANJANA VIJAYAN

DEPARTMENT OF ELECTRICAL AND ELECTRONICS ENGINEERING

TKM COLLEGE OF ENGINEERING

KOLLAM - 691 005

CERTIFICATE

This is to certify that the report entitled " **Fault Diagnosis of a Launch Vehicle Actuation System using Wavelet Neural Network** " submitted by **ANJANA VIJAYAN** , **(Reg. No. TKM20EEII06)** of fourth semester to the APJ Abdul Kalam Technological University in partial fulfillment of the requirements for the award of the Degree of Master of Technology in Electrical and Electronics Engineering with specialisation in Industrial Instrumentation and Control, is a bonafide record of the project work done by her under our guidance and supervision. This report in any form has not been submitted to any other University or Institute for any purpose.

Prof. Asha Ravindranath
Internal Supervisor
Associate Professor
Department of EEE
TKM College of Engineering

Mr. Baby Sebastian
External Supervisor
Sci/Engr.
SDCD, CESG/AVN
VSSC

Prof. Shanavas T N
PG Coordinator
Associate Professor
Department of EEE
TKM College of Engineering

Dr. Sabeena Beevi K
Head of the Department
Associate Professor
Department of EEE
TKM College of Engineering

Prof. Sumayya Jaleel
Project Coordinator
Assistant Professor
Department of EEE
TKM College of Engineering

Acknowledgement

A lot of effort and hard work has been put into this project in course of its presentation. However, it would not have been possible without the kind support and help of many individuals and other sources. I would like to extend my sincere thanks to all of them. I take this opportunity to express my deep sense of gratitude and sincere thanks to all who helped me to complete this project report successfully.

I express my sincere gratitude to Principal *Dr. T A Shahul Hameed* for providing all necessary facilities.

I am indebted to *Dr. Sabeena Beevi K*, Head of the Department, Dept. of EEE, *Dr. Imthias Ahamed T P*, Professor, TKM College of Engineering, and *Prof. Shanavas T N*, PG Coordinator, Dept. of EEE, for their valuable guidance and suggestions to make this work a great success.

I am greatly thankful to my internal guide *Prof. Asha Ravindranath*, Associate Professor, Dept. of EEE, and my external guide *Mr. Baby Sebastian*, Sci/Engr., VSSC, for their excellent guidance, positive criticism and valuable comments.

I express my gratitude to Project Coordinator *Prof. Sumayya Jaleel*, Assistant Professor, Dept. of EEE, and *Prof. Amal A.*, Assistant Professor, Dept. of EEE, for all the guidance and encouragement in the fulfilment of this work.

Finally, I thank my parents, friends, near and dear ones who directly and indirectly contributed to the successful completion of my project work.

ANJANA VIJAYAN

Abstract

Small Satellite Launch Vehicle (SSLV) is a four-stage launcher that is being developed by the Indian Space Research Organization (ISRO) for launching small satellites and has the potential to enable multiple orbital drop-offs. Of the four stages, three of them are solid propellant stages that used the Flex Nozzle Control (FNC) system for controlling the deflection of the rocket nozzle. FNC system uses Electromechanical Actuators (EMAs) for closed loop position control in the pitch and yaw axis of SSLV.

Fault diagnosis is a critical problem in spacecraft operations in terms of performance, safety, and reliability. Feature extraction for the generation of the dataset is done using Wavelet Transform (WT). A fault classifier based on Wavelet Neural Network (WNN) is used for the diagnosis of five system conditions. When compared with the conventional artificial neural network (ANN), WNN considers the fault type comprehensively and provides more accurate results. The modeling of launch vehicle actuation system and the fault classifier network was evaluated in the MATLAB environment.

Contents

List of Tables

List of Figures

Abbreviations

ANN	Artificial Neural Network
BLDC	Brushless DC
CWT	Continuous Wavelet Transform
DWT	Discrete Wavelet Transform
EGC	Engine Gimbal Control
EMA	Electromechanical Actuator
FNC	Flex Nozzle Control
FT	Fourier Transform
ISRO	Indian Space Research Organisation
LEO	Low Earth Orbit
LPF	Low Pass Filter
MI	Moment of Inertia
MSE	Mean Square Error
PI	Proportional Integral
PWM	Pulse Width Modulation
SITVC	Secondary Injection Thrust Vector Control
SSLV	Small Satellite Launch Vehicle
SSO	Sun Synchronous Orbit
VTM	Velocity Trimming Module
WPT	Wavelet Packet Transform

WNN Wavelet Neural Network

WT Wavelet Transform

Notations

B_N	Nozzle viscous damping coefficient
B_m	Viscous damping of BLDC torque motor
F_c	Coulomb Friction Coefficient
J_m	MI of torque motor rotating assembly
J_N	Engine Moment of Inertia
K_A	Net power amplifier gain
K_b	Motor back emf constant
K_{cf}	Feedback gain of current loop
K_l	Actuator mounting structure stiffness
K_N	Stiffness of flex seal
K_p	Scale factor of position sensor
K_t	Motor torque sensitivity
l_m	Actuator lever arm length
n_b	Ball screw gear ratio
N_{ch}	Number of operating channels of motor
V_i	Power amplifier input voltage
V_s	Voltage applied across the motor coil
Z_m	DC torque motor coil impedance per coil

Chapter 1

INTRODUCTION

1.1 Overview

A launch vehicle is used to carry a payload to or beyond Earth's orbit. The payload can be satellite, spacecraft, rovers etc. The classification of launch vehicle is basically done based on the payload capacity.

1.1.1 Small Satellite Launch Vehicle (SSLV)

SSLV is a launcher that is being developed by the Indian Space Research Organization (ISRO). It has the ability to launch multiple satellites into low earth orbit (LEO) or sun-synchronous orbit (SSO). It can launch satellites weighing up to 500 kg into a 500km planar orbit. SSLV has three solid propulsion stages and a liquid Velocity Trimming Module (VTM) as the terminal stage [6].

The salient features of SSLV are [10]:

1. Multiple satellites can be accommodated with ease
2. Low cost and less turn-around time
3. Feasibility of launching on demand
4. Infrastructure requirements for launch are minimum
5. Increased production rate from industries

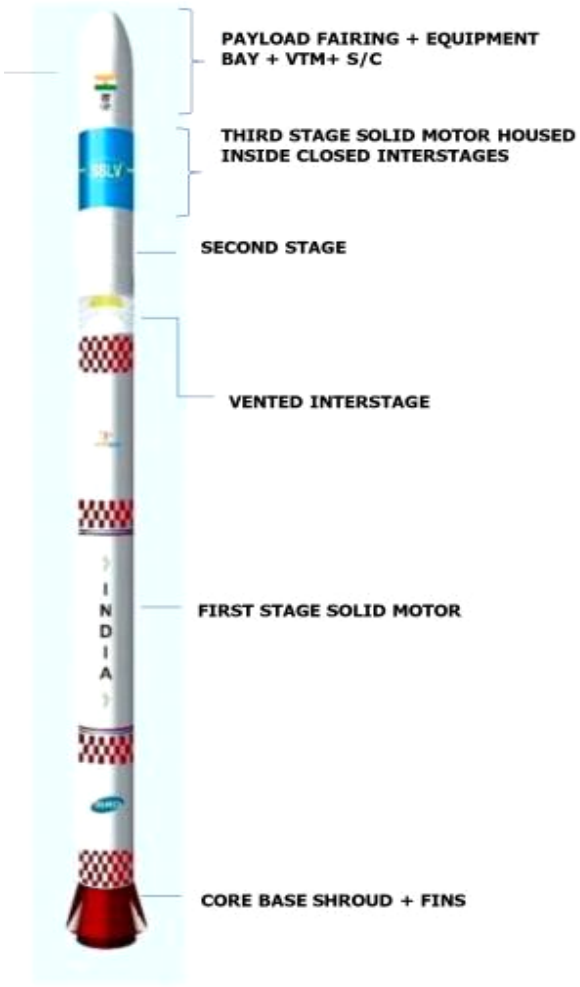

Figure 1.1: SSLV

The vehicle has a height of 34 metres, a diameter of two metres, and a lift-off mass of 120 tonnes. SSLV is a good and affordable choice since it can be put together in a few days by one smaller team for a far lower cost than PSLV. The SSLV can be built horizontally, just like decommissioned SLV and ASLV, or vertically, like the current PSLV and GSLVs. Fig. 1.1 [10] shows the small satellite launch vehicle configuration.

1.1.2 Flex Nozzle Control (FNC) System

Thrust vectoring achieved by deflection of just the rocket's nozzle in solid fuel ballistic missiles and solid rocket motors. Flex Nozzle Control (FNC) is the term for this. Due to its design simplicity and reliability, FNC is chosen over alternative approaches such as Secondary Injection Thrust Vector Control (SITVC). A flexible joint design with a flexible part called the flex seal

as well as a couple of actuators, together referred to as the flex nozzle system, is used in most FNC systems (FNS) [2]. During flight, the associated control electronics assist in meeting the actuation needs. A cylindrical body containing spherical iron shims with elastomers stacked in alternating layers is used for flex seals [3]. The schematic diagram of FNC system is shown in Fig. 1.2 [6].

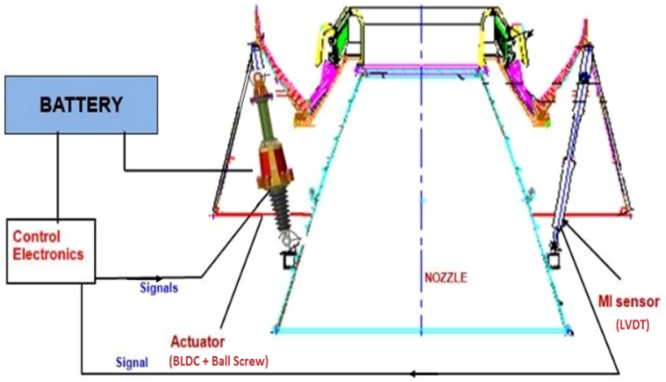

Figure 1.2: FNC system

1.2 Motivation

All components are supposed to perform properly and accurately in control theory. System components may experience problems or failures on a regular basis. Fault detection has become extremely relevant area as the demand for a safe and dependable controller grows.

Wavelet Transform is a strong tool used for feature extraction from the system. Wavelet neural networks combine the capabilities of wavelet decomposition with neural network performance. With a smaller network size, the accuracy of the approximation can be comparable to a feed-forward network. The wavelet function will be used as the activation function for hidden nodes in wavelet neural networks.

1.3 Objectives

The objectives of the work includes the following :

1. To model linear and non-linear launch vehicle actuation system

2. To identify the commonly occurring faults in the system and use wavelet transform for feature extraction

3. Classify the faulty and healthy system using Wavelet Neural Network

1.4 Organization of Report

The report is organised as follows :

- Chapter 2 is the literature review, where the background study of the system and methodology is done
- Chapter 3 constitute the modeling of linear and nonlinear launch vehicle actuation system
- The feature extraction methodology and the classifier design is done in chapter 4
- Results obtained from simulation of the model and the classifier using MATLAB/SIMULINK is explained in chapter 5
- Chapter 6 is the conclusions of the work

Chapter 2

LITERATURE REVIEW

2.1 Launch Vehicle Actuation System

Thrust vector control (TVC) is the manipulation of the path of thrust from a rocket's or other vehicle's engines in order to regulate the vehicle's attitude or angular velocity [9]. In the context of rockets, missiles, and other vehicles that fly beyond the atmosphere, aerodynamic steering control elements are useless, leaving thrust vectoring as principal means of attitude control. Whenever the propulsion system generates thrust, TVC is achievable. During various stages of flight, technologies other than TVC are required for attitude control and flight path control. Thrust vectoring was previously achievable with hydraulic actuators in thrust vector control systems. This has been replaced by the electromechanical actuators since they are reliable and has lesser maintenance.

The launch vehicle actuation system of SSLV has BLDC torque motor as the main driving element [5]. The main driving element is a BLDC torque motor, and closed loop position control is achieved through a ball screw mechanism. Nozzle angular position is sensed by LVDTs and compared to the voltage equivalent to the intended position. The error signal generated is amplified, corrected, and sent to the BLDC torque motor.

The compensation scheme is designed as per the system requirements [7]. In the forward path, a lead compensator has been employed. This has the potential to boost the system's gain at high frequencies, which is undesirable. As a result, the stability margin is reduced. A rate filter is employed instead of a lead compensator, which serves the same purpose but does not boost gain. A lag compensator is similar to an LPF. It enhances steady-state performance by allowing

high gain at lower frequency region while limiting gain at higher frequencies to increase phase margin. Steady state error is also reduced.

2.2 Wavelet Transform

Slowly varying trends or oscillations punctuated with transients are common in real-world data or signals. But, some signals show abrupt changes rather than the smooth regions as in an image signal. These parts carry important information about the signal. The Fourier transform (FT) is a spectral analysis technique that decomposes a function into a sum of sine waves of various frequencies. Since FT represents the signals as the sum of sine or cosine waves, it cannot be localized in time or space. It is more suitable for stationary signals and cannot represent the abrupt changes in the signals that contain important data. For analysis of signals which have abrupt changes, wavelets are used. WT is a suitable analysis method that is well-known for its ability to extract features for machinery fault detection.

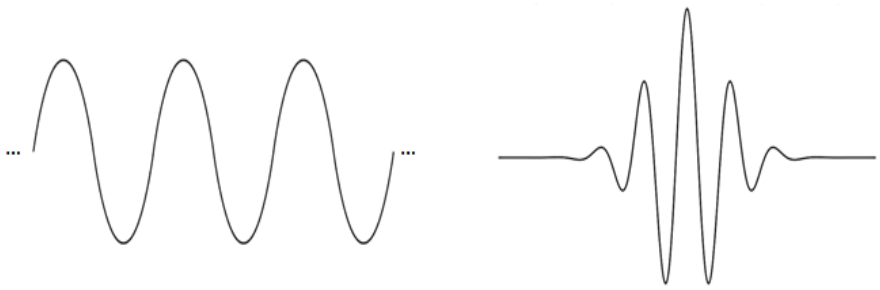

Figure 2.1: Sine wave and Wavelet

2.2.1 Wavelet

The wavelet is a fast decomposing wave like an oscillation which has a zero mean. Wavelets are having finite duration unlike sinusoids. In Fourier analysis, a signal is split into sine waves of various frequencies. In contrast, wavelet analysis divides a signal into scaled and shifted copies of the mother wavelet. From Fig. 2.1 of sine wave and wavelet, it's clear that signals with sharp changes would benefit from an irregular wavelet rather than a smooth sinusoid.

To be classified as a wavelet, a function (ψ) defined over the real axis ($-\infty, \infty$) must have the following three properties:

- The integral of ψ equals 0:

$$\int_{-\infty}^{\infty} \psi(u)\, du = 0 \tag{2.1}$$

- The integral of the square of ψ is unity:

$$\int_{-\infty}^{\infty} \psi^2(u)\, du = 1 \tag{2.2}$$

- Admissibility Condition:

$$C_\psi = \int_0^{\infty} \frac{|\psi(f)|^2}{f}\, df \quad satisfies \quad 0 < C_\psi < \infty \tag{2.3}$$

2.2.2 Continuous Wavelet Transform (CWT)

The CWT is a non-numerical method that gives the signal representation by allowing the wavelet's translation and scale parameters to fluctuate continuously [13], [21].

For a function $x(t)$, the CWT at a scale ($a > 0$) and the translational value ($b \in \mathbb{R}$) can be represented as,

$$F(a,b) = \frac{1}{\sqrt{|a|}} \int_{-\infty}^{\infty} x(t)\, \psi^* \left(\frac{t-b}{a} \right) dt \tag{2.4}$$

In eqn. 2.4, $\frac{1}{\sqrt{|a|}}$ is the normalization factor.

The advantage of CWT is that it allows for signal processing at an intermediate scale within each octave. The number of scales per octave is the deciding parameter. The finer the scale discretization, the more scales per octave there are.

When it comes to estimating the damping ratio of oscillating signals, CWT is quite effective. CWT is also extremely robust to signal noise. In the CWT, there are many alternatives in wavelets that is used. While the fact that there is more options for evaluating wavelets may appear complicated, in fact, wavelet analysis has this advantage.. A specific wavelet can be chosen, that helps to detect the signal properties based on what is to be detected [19].

2.2.3 Properties of Wavelet

The analyzing function in the CWT is a wavelet. In CWT, it compares the signal to wavelets that have been moved, compressed, or stretched. Dilation or scaling refers to the process of stretching or compressing of a function, and it corresponds to physical concept of scale.

(i) **Scaling**

A signal's scale factor "a" dilates or compresses it. When the scale factor is low, the signal is compressed, resulting in a more detailed graph. The low scale factor, on the other hand, doesn't last for the entire duration of the signal. When the scale factor is high, however, the signal is stretched out, resulting in a less detailed graph. Nonetheless, it frequently lasts the entire signal duration. The wavelet becomes more compressed as the scale factor decreases. Conversely, the wavelet becomes more stretched as the scale increases.

Figure 2.2: Scaling property of wavelet

There is a definite connection between scale and frequency. More stretched wavelets correspond to the longest scales. Longer the signal section with which the wavelet is compared, finer is the signal features measured from the wavelet coefficients and the wavelet becomes more stretched. A wavelet function and its scaled signal is shown in Fig. 2.2.

(ii) **Shifting**

Delaying (or advancing) the appearance of a wavelet is referred to as shifting. Delaying a function $x(t)$ by b is represented mathematically by $x(t-b)$.

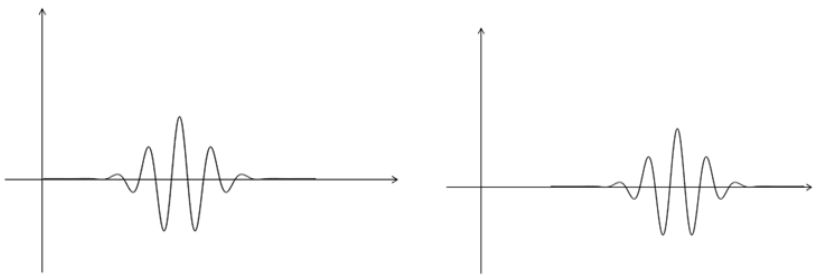

Figure 2.3: Shifting property of wavelet

Wavelets, unlike waves, are only non-zero for a limited period of time, hence location is crucial. Furthermore, when studying a signal, the interest is not only in its oscillations, but also in where they occur. A wavelet function and its delayed signal is shown in Fig. 2.3.

2.2.4 Discrete Wavelet Transform (DWT)

If calculations on several scales are to be made while executing CWT, it will end up with a lot of calculations and a low computational efficiency. DWT is used to tackle this problem. DWT can be represented as,

$$DWT(y,z) = \frac{1}{\sqrt{y}} \int_{-\infty}^{\infty} f(t)\, \psi^* \left(\frac{t-z}{y} \right) dt \tag{2.5}$$

where $y = 2^j$ and $z = k2^j$

Sampling is done at a base scale of 2 [16]. It's ideal for denoising and compression of signals and images since it reduces the number of coefficients needed to represent various naturally occurring signals and images. DWT requires lesser memory.

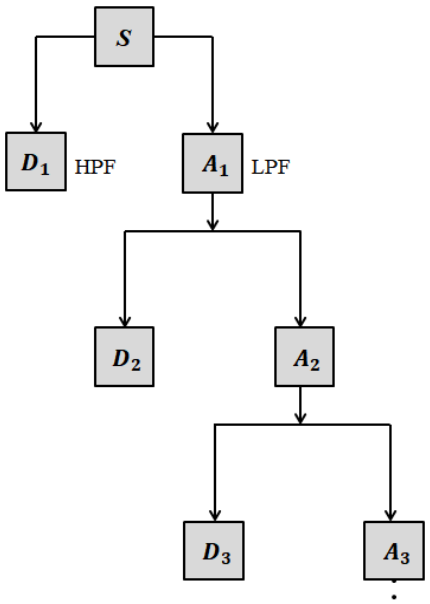

Figure 2.4: Discrete Wavelet Transform

The decomposition tree after DWT is shown in Fig. 2.4. After filtering, according to the Nyquist criterion, half of the samples are eliminated [28].

2.2.5 Wavelet Packet Transform (WPT)

The discrete-time (sampled) signal is passed through more filters in the WPT than in the DWT. To generate the whole binary tree, the WPT decomposes both the detail and approximation

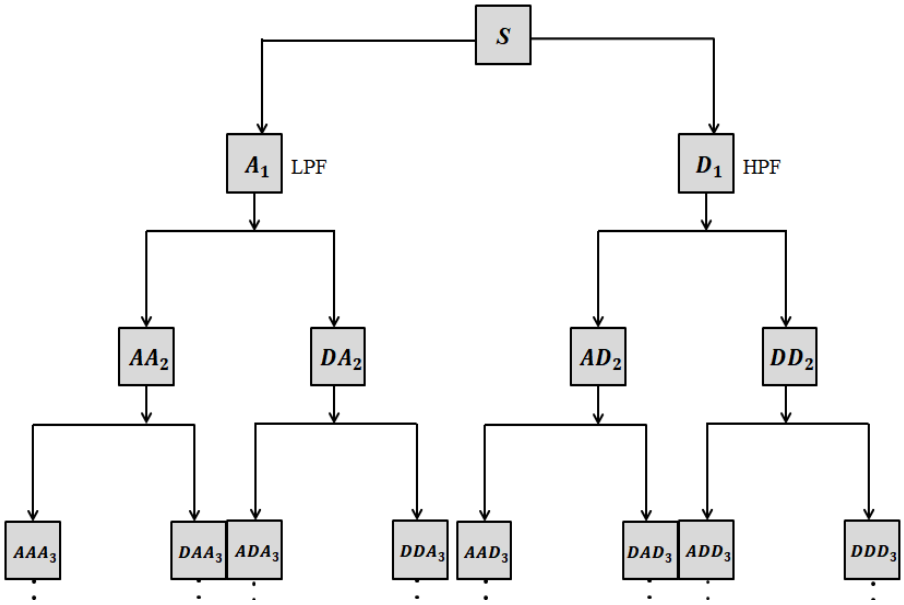

Figure 2.5: Wavelet Packet Transform

coefficients [15], shown in Fig. 2.5.

2.2.6 Wavelet Family

Orthogonal wavelets (Daubechies extremal phase and least asymmetric wavelets) and B-spline which are bi orthogonal wavelets are examples of wavelets used for DWT. Wavelet families differ in a number of ways:

- Support for the wavelet in terms of time, frequency, and decay rate
- The wavelet's symmetry or anti symmetry
- The wavelet's regularity
- The scaling function existence

Some of the commonly used wavelets are:

(i) **Haar Wavelet**

Fig. 2.6 shows the haar wavelet. It is a avelet with a compact support. The most basic and

oldest wavelet.

The wavelet function $\psi(t)$ can be represented as:

$$\psi(t) = \begin{cases} 1 & 0 < t < \frac{1}{2} \\ -1 & \frac{1}{2} \leq t < 1 \\ 0 & \text{otherwise} \end{cases} \tag{2.6}$$

The scaling function $\phi(t)$ is given by:

$$\psi(t) = \begin{cases} 1 & 0 \leq t < 1 \\ 0 & \text{otherwise} \end{cases} \tag{2.7}$$

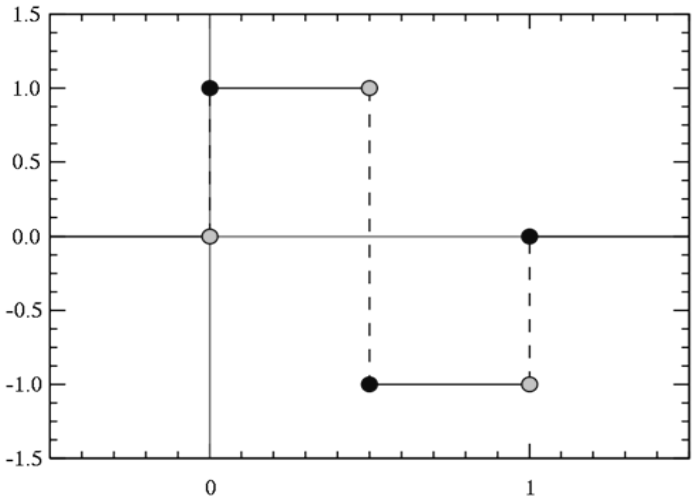

Figure 2.6: Haar Wavelet

It is symmetric. But has the technical disadvantage of not being continuous and hence not differentiable. This characteristic, on the other hand, might be advantageous in the analysis of data with abrupt transitions (discrete signals), such as machine tool failure monitoring.

(ii) **Daubechies Wavelet**

Daubechies extremal phase wavelets are known as dbN wavelets. The number of vanishing moments is denoted by the letter N. In the literature, these filters are also referred to by the number of filter taps, which is 2N. Daubechies wavelets are commonly used to solve a variety of difficulties, including signal self-similarity traits, fractal problems, signal discontinuities, and so on. Fig. 2.7 shows the daubechies wavelet and its scaling function.

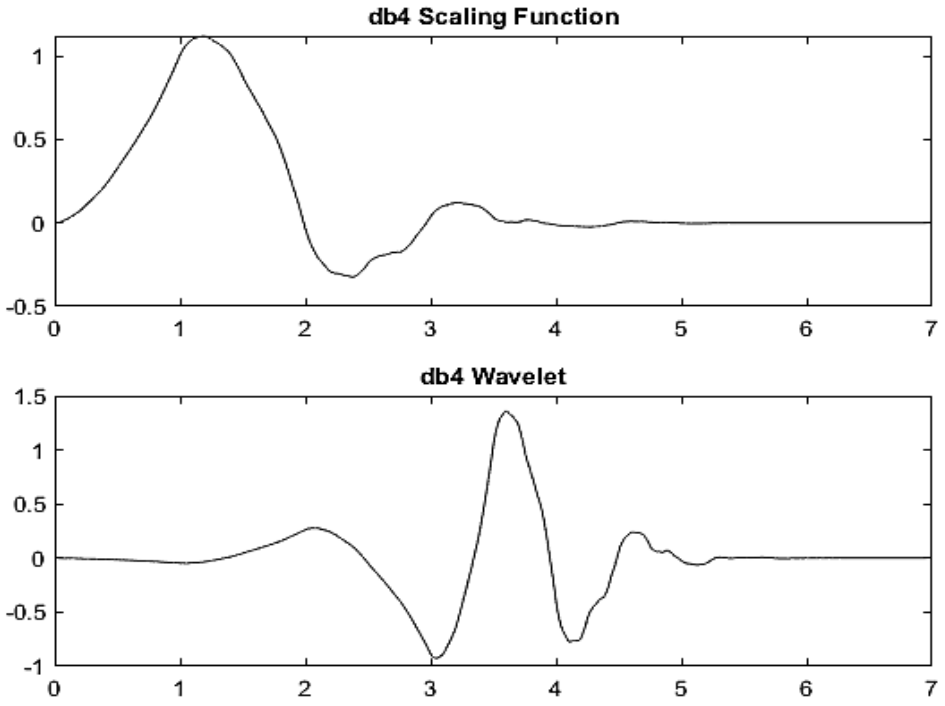

Figure 2.7: Daubechies Wavelet

(iii) **Mexican hat Wavelet**

It is also called as Ricker wavelet. It's a subset of the continuous wavelet family. This wavelet has no scaling function. The wavelet is depicted in Fig. 2.8.

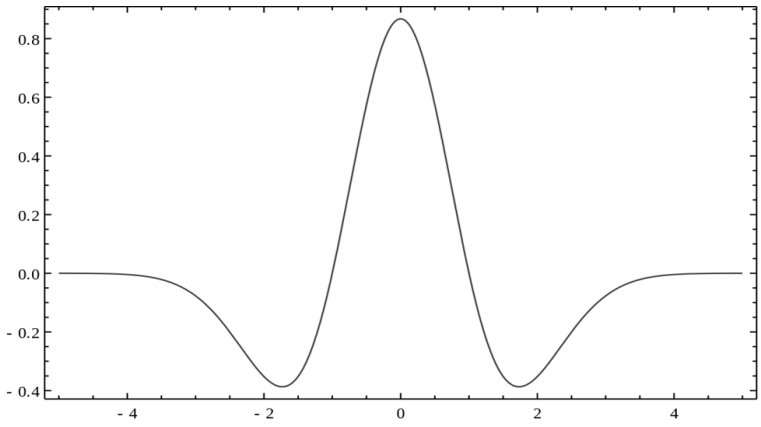

Figure 2.8: Mexican hat Wavelet

(iv) **Morlet Wavelet**

This wavelet is available in both real- and complex-valued variants. Morlet is a cosine-modulated Gaussian wavelet with the benefit of high time-frequency resolution [20].

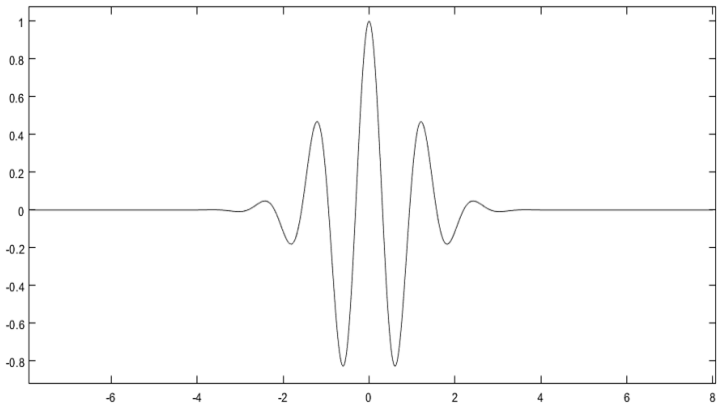

Figure 2.9: Morlet Wavelet

2.3 Neural Network

With their extraordinary capacity to infer meaning from complex or imprecise data, neural networks might be used to uncover patterns and discover trends that are too complex for people or other computer systems to notice.

2.3.1 Artificial Neural Network

ANNs are made up of a huge number of interconnected processing elements known as nodes, units, or neurons, which function in parallel and are organized in regular topologies. ANN's main goal is to generalise its learned information to similar but unknown input patterns. A connecting link connects one neuron to the others. One of an ANNs main goals is to generalize its learned information to similar but unknown input patterns. A connecting link connects each neuron to the next. Weights containing features of the input signal are connected with each connection link. The neural network uses this data to tackle a specific problem. The ability of ANNs to learn, recall, and generalize training patterns or data, comparable to that of a human brain, characterizes their collective behavior. They have the ability to model networks similar to those found in the brain. The processing parts of ANNs are referred to as neurons or artificial neurons [13], [29].

The net input in the model shown in Fig. 2.10 is defined as in eq. 2.8.

$$y_{in} = x_1w_1 + x_2w_2 + x_3w_3 + ... + x_nw_n = \sum_{i=1}^{n} x_iw_i \tag{2.8}$$

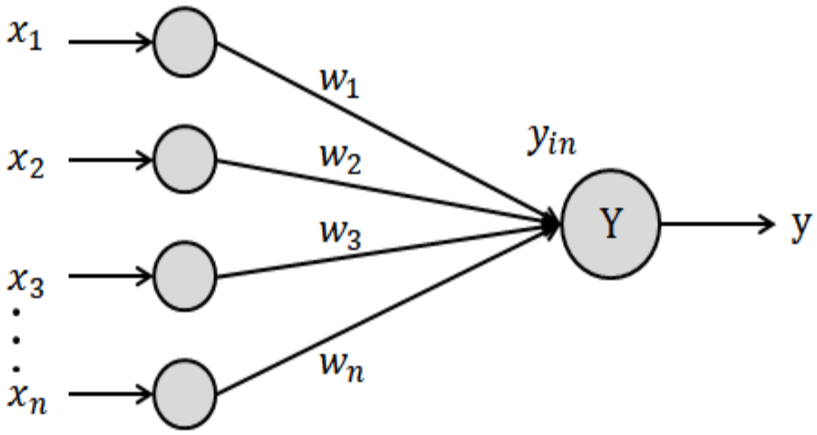

Figure 2.10: Architecture of ANN

where, x_1, x_2,..x_n are the activations of input neurons and w_1, w_2..w_n are the input weights. By applying activations over net input, output is obtained, which is given by:

$$Output = f(y_{in}) \tag{2.9}$$

A neural network's elements include:

(i) **Input Layer**

The database's raw input is sent into the input nodes. This layer does not do any computations. The information (features) is simply passed on to the hidden layer via the nodes in this layer.

(ii) **Hidden Layer**

The hidden layer computes all of the features input from the input nodes and sends the results to the output layer.

(iii) **Output Layer**

The output layer of a neural network is the outer layer of neurons that generates the program's outputs.

(iv) **Bias**

The role of bias in neural networks may be compared to that of a constant in a linear equation.

(v) **Activation Functions**

The activation function of a node specifies the node's output in response to a single or many inputs. An activation function is being used to bring a neural network non-linearity. Some of the commonly used activation functions are:

- Identity
- Sigmoid
- Hyperbolic tangent
- Binary step
- Rectified linear unit

(vi) **Learning Rate**

The learning rate determines how large the model's corrective steps are in adapting to faults in each observation. A high learning rate reduces training time but reduces overall accuracy, whereas a low learning rate takes longer but has the potential for better accuracy.

(vii) **Cost Function**

A cost function is a critical factor that defines how well a model works on a particular dataset. It calculates and expresses the difference between the expected and forecasted values as a single real number.

Advantages of AANs are:

- The cycle time of execution in an ANN is nanoseconds, whereas it is a few milliseconds in a normal neuron. As a result, the computer-modeled artificial neuron is faster.
- The artificial neuron network method is significantly faster than the biological neuron's processing
- An ANN's computing capacity is usually unaffected by damage to a single component

2.3.2 Wavelet Neural Network

A feed-forward neural network with one or more inputs, hidden layer, and summers at the output layer. The neurons in the hidden layer have activation functions taken from a wavelet basis. Wavelons are the common name for these wavelet neurons. The following processes precede wavelet neural network modeling:

- Wavelet neural network structure selection
- Configuring the network settings
- Training of wavelet neural network

One of the most used approaches in supervised learning is backpropagation based on the gradient descent method that enhances the speed of wavelet neural network. Fig. 2.11 shows the architecture of WNN.

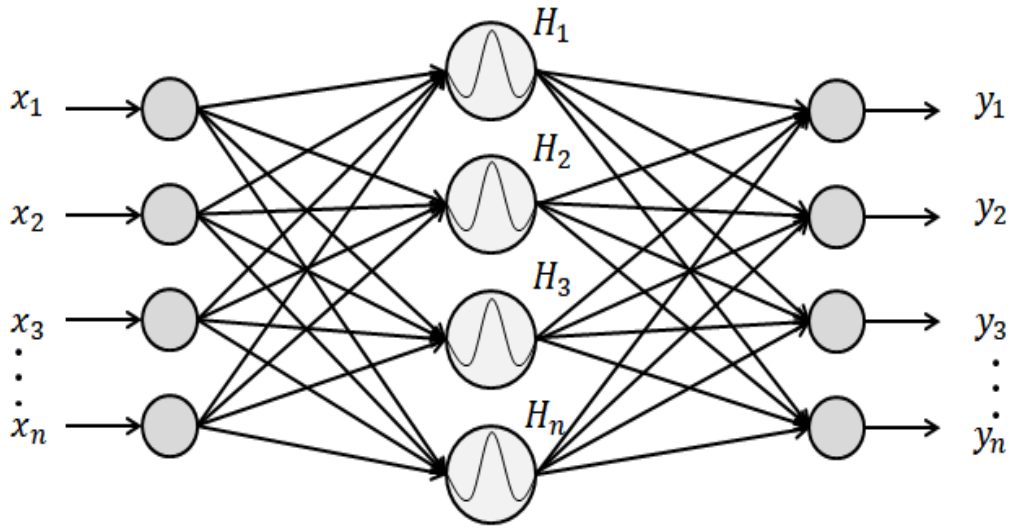

Figure 2.11: Architecture of WNN

2.4 Backpropagation

For training multi-layer perceptrons, backpropagation is a supervised learning technique. In the testing phase, the obtained output in the first iteration may not be the desired output. As a result,

more iterations are to be done. Iterations improve accuracy and improve error since weight is being updated after every iteration [23].

Gradient descent is a regularly used approach to determine the weights that minimises the error. The steepest descent direction of the loss function vs the current synaptic weights is computed via backpropagation. The weights may then be adjusted in the steepest descent path, resulting in an effective error minimization.

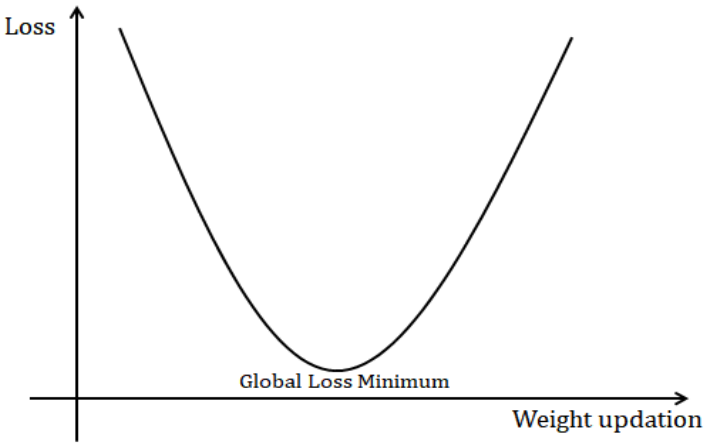

Figure 2.12: Gradient Descent Optimization

After a training example has passed through the network, the loss function/cost function estimates the difference between the output of the network and the predicted output.

2.5 Faults in actuation system

A fault is defined as a deviation from a nominal behaviour in one or more distinctive attributes of a system variable. It also results in poor system performance. Once the issue diagnosis is complete, a remedy must be designed to restore the system to its desired performance levels [7].

Although EMAs are relatively new to the aerospace field, the notion of all electric aircraft and spaceship designs suggests that EMAs will replace hydraulic actuators in the future. EMAs were employed in spacecraft for things like antenna alignment and robotic arm movement. EMAs are increasingly used for thrust vector control in rocket launcher systems. Actuator failure that goes unnoticed might have severe impacts.

The FNC actuation system's defects are divided into four categories: sensor, mechanical or structural, motor, and power or electrical.

2.5.1 Sensor faults

Sensor failure identification in dynamic systems has typically relied on hardware redundancy, which involves the use of more than two sensors to measure the same variable. Sensors that are either entirely or partially failing give inaccurate monitoring and control information [17]. Following are the general sensor faults in EMA system:

(i) **Bias**

Even if there's no mobility, there is a slight offset in the average signal output. This is referred to as Sensor Bias, depicted in Fig. 2.13.

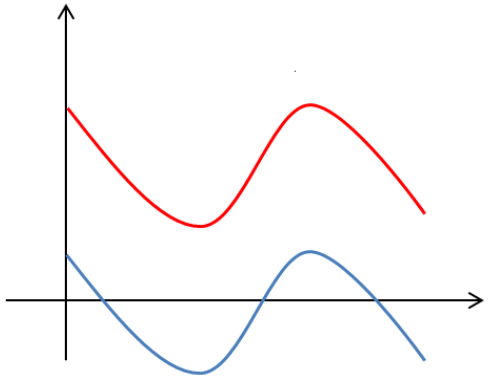

Figure 2.13: Sensor bias

(ii) **Drift**

Gradual shift in the measurement over time. 29% mean value change over the nominal value reported at the end of the drift is considered as fault.

(iii) **Noise**

Sensor noise is the result of individual changes in the sensor output that are independent of changes in sensor input. The median considered as a fault is 20% peak to peak value over the nominal value.

(iv) **Scaling**

The constants of proportionate relationship between the input and output are referred to as scale factor error. Variation of the sensor's sensitivity from its ideal one.

2.5.2 Mechanical/Structural faults

Excessive loads, environmental conditions, lubrication difficulties, and manufacturing faults are the major reasons. Some of the significant mechanical fault conditions are listed in Table 2.1 [12].

Table 2.1: Major structural faults

Component	Fault	Failure
Screw	Excessive wear	Metal flakes separation and extreme vibrations
Nut	Bent	Seizure
Bearings	Corrosion	Separation and strong tremors
Balls	Excessive wear	Backlash
Mountings	Cracks	Complete Failure

2.5.3 Motor faults

Motors are frequently run at high rotational speeds, which causes increased temperature and mechanical stress and thus experience winding shorts, rotor shaft eccentricities, and other issues. Table 2.2 [12] shows major motor faults.

Table 2.2: Motor faults

Component	Fault	Failure
Stator	Stator coil fault, Insulation deterioration	Short Circuit
Rotor	Rotor eccentricity	Support bearing failure
Connectors	Intermittent Contact	Disconnection

2.5.4 Power/Electrical faults

Electrical and electronic failures in EMAs power and control systems seem to be the same in comparison to similar sort of flaws in other aerospace systems. Table 2.3 shows major electrical faults in EMA system.

Table 2.3: Electronic faults

Component	**Fault**	**Failure**
Wiring	Short circuit, Open circuit, Insulation Failure	Short circuit, Open circuit
Solder joints	Intermittent contact	Disconnection
Power supply	Short circuit, Open circuit	Short circuit, Open circuit

2.6 Concluding Remarks

This chapter dealt with the literature survey done. The referenced works offer a foundation for the development of new work that takes into account the most recent trends and advancements in the field of fault detection in EMA systems.

Chapter 3

MODELING OF FNC SYSTEM

3.1 System Description

Launch vehicle control during the ascent means the ability to control the vector of thrust produced. Thrust Vector Control (TVC) or Thrust Vectoring is used in launch vehicles to control the attitude [9]. It is controlled by changing the engine's thrust direction.. TVC uses the thrust generated from the propulsion system and is effective in controlling the direction of flight for a launch vehicle that fly outside Earth's atmosphere. Within the Earth's atmosphere, flight control surfaces can control the direction of flight [6]. FNC is a form of TVC that provides precise steering of launch vehicle. This is done by using servo actuation system.

The launch vehicle can be steered in pitch, yaw and roll directions. The actuators used for this purpose can be linear or rotary based on the required deflection. Linear actuators provide small engine deflection ($\pm 4^{\circ}$) [9]. For greater deflection, rotary actuators are preferred. Linear actuators can be fluid powered and motor powered. Pneumatic and hydraulic actuators are fluid powered while electromechanical actuators (EMA) are motor powered. EMA's are used instead of hydraulic actuators as hydraulic actuators are larger in size and weight. Also by using hydraulic actuators, it is difficult to avoid leaks and give reliable performance. EMA's have the following advantages compared to hydraulic actuators [1].

- Simple configuration
- Reduced system weight
- Reduced cost

- Easy isolation and fault detection scheme
- Lesser number of components
- Less lead time for flight readiness
- No launch count down operations

While selecting the actuators for launch vehicle application, it should be of reduced weight and size and should also be reliable.

The electromechanical actuation system used is based on BLDC torque motor [8]. The system uses two linear and independant EMA's placed orthogonally to actuate the nozzle. The BLDC torque motor is powered from a DC source. The motor gives essential torque about the nozzle pivot. The torque motor output is given to the ball screw mechanism. This converts the rotary motion of motor to translational motion. The drive mechanism converts translational motion to corresponding angular motion of engine. Since the one end of actuator is connected to the nozzle, it induces a corresponding deflection.

The nozzle deflection is measured using two potentiometers which is mounted at 180° with respect to each other. One sensing element (main potentiometer) is placed inside the actuator. The other one is called the mirror potentiometer. The difference in sesnsed outputs from main and mirror potentiometer is given as the position feedback signal. The position feedback signal is then compared with the input command to obtain the error signal. The error signal is compensated and then amplified using PWM type power amplifiers. and supplied to BLDC torque motor.

A high gain current loop (bandwidth of few kHz) is provided around the amplifier to ensure linear amplifier characteristics and to reject power supply variations.

3.1.1 BLDC Torque Motor

An FNC system's electromechanical actuator consists of a Quadruplex BLDC Motor as an electrical component that supplies rotational motion and then a ball screw that transforms the rotary motion to translational motion [4]. The ball screw is linked to the motor through an appropriate gearing arrangement. The Quadruplex BLDC motor offers the actuator a high level of redundancy. For improved vehicle safety and mission fulfillment, effective identification and separation of sensor defects in actuation systems are required.

For aerospace applications, a torque motor with improved position stability, better torque density, low cogging torque, and higher torque to inertia ratio is required. Brushless DC motors (BLDC) are more dependable, easier to regulate, and economical, in addition to having improved speed vs torque characteristics, good dynamic responsiveness, higher efficiency, extended working life, noiseless operation, and larger speed ranges [1], [14]. Because of their good electrical and mechanical qualities, BLDC motors are frequently employed in aircraft applications.

3.1.2 Ball Screw

Linear actuators are responsible for translating an electric motor's rotating motion into linear motion [1]. The linear actuator in a FNC system features a casing with a BLDC motor, a gear system for speed reduction, and a ball screw mechanism for accurately translating the rotating motion of a BLDC motor shaft into linear motion of a driving shaft.

A ball nut, ball screw shaft, nut housing, and end bearings make up the ball screw assembly. The ball screw shaft gets placed into the ball nut by a number of ball bearings that are recirculated within the nut on a continual basis. In rotation, its ball screw shaft remains held on the housing, however,it cannot move axially. The speed restriction mechanism includes an output gear configuration, which is mounted on the nut. The ball bearings allow the screw to revolve within the nut with little frictional loss, allowing it to operate at faster speeds and for longer periods of time without overheating. The ball bearings are mounted on a shaft with a helical ball track.

3.1.3 Nozzle

Nozzles are essentially ducts with different cross-sectional areas. The thermodynamic expansion of a nozzle converts thermal energy generated by chemical, electrical, or nuclear sources into kinetic energy. When a flow travels through a nozzle, it undergoes adiabatic changes in its thermodynamic characteristics. Nozzles are used to change the flow's pressure or velocity in a variety of applications [2], [3].

The nozzle is located at the end of a jet or rocket engine to transfer the thermal energy of the gases in the combustion process to the kinetic energy of the exhaust gas by allowing it to expand. The exhaust extends past its throat until it leaves the nozzle, increasing velocity and

momentum in the process. The force exerted on the gases creates an opposing force operating on the rocket, according to Newton's third law. Nozzles also have the ability to collect and correct the gas flow. The flex nozzle control system, which uses a nozzle with such a flexible joint, is the most developed of the numerous thrust vector control systems available. The direction of exhaust gas flow, and hence the path of thrust with regard to the rocket's centre of gravity, changes as the nozzle moves. To deflect the nozzle and change the trajectory of the rocket engine's thrust vector, a basic FNC system uses a flexible joint design with a flex seal as well as a pair of actuators [11].

3.1.4 LVDT

The Linear Variable Differential Transformer (LVDT) is a type of transducer that transforms a linear displacement or position into a proportional electrical signal including phase and amplitude information. The produced output is proportionate to the position of the moveable magnetic core. Inside a transformer with a central primary coil and two exterior secondary coils arranged in a cylindrical form, the magnetic core flows linearly.

An AC voltage source excites the primary winding, causing voltages in the secondary to change depending on the location of the magnetic material inside the assembly. The object for which the displacement is being recorded is connected to a non-ferromagnetic rod. The LVDT's core is frequently threaded to make a connection to this non-ferromagnetic rod easier. The secondary coils are wound in such a way that the voltages generated within two secondary windings opposed each other when the core is centred, resulting in a net output voltage of zero. When the LVDT's core is pushed away from the center, the voltage within the secondary coil to which the core is moving rises whereas the voltage in other secondary winding falls.

The LVDT's frictionless functioning is a key characteristic. In highly reliable applications such as airplanes, satellites, space vehicles, nuclear sites, and so on, LVDT is preferred. The FNC system's measuring system comprises of LVDT providing position measurement. For measuring the deflection of the rocket nozzle, a triplex redundant LVDT was mechanically linked with it. The angular displacement from LVDT is compared to a volt equivalent to the required displacement, which is sent to the system as command input. After adjustment, the resultant error voltage is magnified and sent to the BLDC motor, which generates the needed torque around the nozzle pivot to cancel the erroneous signal.

3.2 Mathematical Modeling of Linear FNC System

The mathematical modeling of the Linear FNC system is done in this section. The modeling of BLDC motor, nozzle, ball screw arrangement, and LVDT is done.

3.2.1 BLDC Torque Motor

The torque motor used in the FNC system is approximated as a second order linear system. The dynamics of the BLDC motor is given in eq. 3.1.

$$\begin{aligned} J_m\dot{\omega}_m + B_m\omega_m &= T_e - T_L \\ J_m\ddot{\theta}_m + B_m\dot{\theta}_m &= T_e - T_L \end{aligned} \tag{3.1}$$

where, J_m - Moment of inertia of the torque motor assembly

B_m - Viscous damping of torque motor

θ_m - Motor angular position

ω_m - Motor speed

T_e - Generated torque

T_L - Load torque

Taking Laplace transform, the transfer function of the motor is obtained as,

$$\begin{aligned} G_m(s) &= \frac{T_e(s) - T_L(s)}{\theta_m(s)} \\ &= \frac{1}{J_m s^2 + B_m s} \end{aligned} \tag{3.2}$$

3.2.2 Nozzle

For deflecting the nozzle and changing the direction of the rocket engine's thrust vector, a typical FNC system uses a flexible joint design with a flex seal and two actuators. The rocket nozzle used in the FNC system is also approximated as a second order system. The governing dynamics of the nozzle is as shown in eq. 3.3.

$$J_N\ddot{\delta}_e + B_N\dot{\delta}_e + K_N\delta_e = T_L \tag{3.3}$$

where, J_N - Engine moment of inertia

B_N - Engine viscous damping coefficient

K_N - Flex nozzle stiffness

δ_e - Angular displacement of the nozzle

Taking Laplace transform, the transfer function of the nozzle is obtained as in eq. 3.4,

$$\begin{aligned} G_N(s) &= \frac{T_L(s)}{\delta_e(s)} \\ &= \frac{1}{J_N s^2 + B_N s + K_N} \end{aligned} \tag{3.4}$$

3.2.3 Ball Screw

The rotary motion of the motor is converted to translational motion of a drive rod mechanism using a ball screw. Rotary motion is transformed into linear motion by the interaction of the ball along the ball screw track. The conversion of rotary motion to linear is represented mathematically by eqn. 3.5,

$$x_s = n_b * \theta_s \tag{3.5}$$

where, x_s - Translational displacement of screw

n_b - Ball screw gear ratio

θ_s - Angular displacement of screw

3.2.4 Driving Torque

The net driving torque available to accelerate the motor rotating moment of inertia is given by eqn. 3.6,

$$T_m = T_{gm} - B_m \omega_m - T_{Lm} \tag{3.6}$$

where, T_{gm} - Motor torque

T_{Lm} - Load torque transmitted to motor side

The rotary motor torque is given by,

$$T_{gm} = \frac{V_{in} * N_{ch} * K_T}{K_{cf}} \tag{3.7}$$

where, V_{in} - Power amplifier input voltage

N_{ch} - Number of operating channels of torque motor

K_T - Torque Sensitivity of motor

K_{cf} - Current loop feedback gain

The load torque transferred to the motor side, T_{Lm} is given by,

$$T_{Lm} = F_L * n_b \tag{3.8}$$

where, F_L - Load force transmitted to the motor side

The load force F_L is given by,

$$F_L = \left[\theta_m - \left(\delta_e * \frac{l_m}{n_b}\right)\right] * n_b * K_l \tag{3.9}$$

where, K_l - Equivalent stiffness of actuator mounting structure including all mechanical elements in series with actuator

l_m - Actuator lever arm length

The nozzle driving torque is given by,

$$T_L = F_L * l_m - T_D \tag{3.10}$$

where, F_L - Load force

T_D - Disturbance torque input to the nozzle

3.2.5 LVDT

The main potentiometer output that corresponds to the angular position of motor is,

$$V_{main} = \theta_m * \frac{n_b}{l_m} * \frac{K_p}{2} \tag{3.11}$$

The mirror potentiometer output that corresponds to the nozzle angular position is,

$$V_{mirror} = \delta_e * \frac{K_p}{2} \tag{3.12}$$

where, K_p - Position sensor scale factor

3.2.6 Compensation Scheme

The compensation scheme of FNC system has one analog current loop and digital position and pseudo rate loops. Torque motor uses PWM type power amplifier, which control the current through the motor coil. To obtain a steady current equivalent to the control voltage, a high gain current loop is provided, which removes the nonlinearities in the PWM amplifier. Additionally, it rejects variations in the power supply.

(i) **Notch Filter**

A notch filter is provided in the forward path to suppress the resonant mode. The mechanical resonance between the equivalent stiffness and equivalent mass is derived from the

fundamentals. The resonance frequency is derived as follows,

$$Resonance frequency = \frac{1}{2\pi}\sqrt{\frac{l_m^2 K_l + K_N}{J_{eff}}} \tag{3.13}$$

where, J_{eff} - Effective moment of inertia derived from engine moment of inertia

The effective moment of inertia derived from engine moment of inertia can be obtained by,

$$J_{eff} = \frac{J_{me} * J_N}{J_{me} * J_N} \tag{3.14}$$

where, J_{me} is the reflected MI of rotor to engine side. i.e,

$$J_{me} = J_m * \left(\frac{l_m}{n_b}\right)^2 \tag{3.15}$$

Consider the general form of the Notch filter transfer function,

$$G_n(s) = \frac{s^2 + 2\zeta_n\omega_n s + \omega_n^2}{s^2 + 2\zeta_d\omega_n s + \omega_n^2} \tag{3.16}$$

The three variables that can be changed are ζ_n, ζ_d and ω_n. The depth of the notch is determined by the ratio of ζ_n and ζ_d, and ω_n is the notch's natural frequency.

(ii) **Pseudo Rate Filter**

Pseudo rate derived from the position sensor output is provided to increase the relative stability of rigid body servo mode [4]. The general transfer function of pseudo rate filter is given by,

$$G_r(s) = \frac{K_r s}{s + \omega_r} \tag{3.17}$$

The value of ω_r is selected such that the bandwidth of the rate loop is about four to five times that of the position loop. Increasing the value of the rate feedback coefficient K_r can reduce the overshoot, but it tends to make the system sluggish.

(iii) **PI Controller and Lag Filter**

The load dynamics for FNC actuator is stiffness dominated with inertia. The damping of the FNC system is relatively very high compared to Engine Gimbal Control (EGC) system. A PI controller with adequate gain and a lag filter are provided in the position loop to reduce the steady state error and to achieve better tracking.

The transfer function of position loop compensator is,

$$G_p(s) = K_p * \left[1 + \frac{K_i}{s}\right] \tag{3.18}$$

The transfer function of lag filter,

$$G_{lg}(s) = K_{lag}(s) * \left[\frac{s+z}{s+p}\right] \tag{3.19}$$

The transfer functions of compensation filters used is shown in Table 3.1.

Table 3.1: Compensation Filters of FNC System

Filter	**Compensator**
Notch Filter	$G_n(s) = \left[\frac{s^2+10.05s+15790}{s^2+125.7s+15790}\right]$
Pseudo rate filter	$G_r(s) = \left[\frac{20s}{s+150}\right]$
PI	$G_p(s) = 6 * \left[1 + \frac{5}{s}\right]$
Lag filter	$G_{lg}(s) = 0.1 * \left[\frac{s+70}{s+14}\right]$

3.2.7 Block Diagram of Linear FNC System

The block diagram of the compensated linear FNC system is given in Fig. 3.1. This model is simulated in MATLAB/SIMULINK and the results are analysed to see if the required specifications have been met.

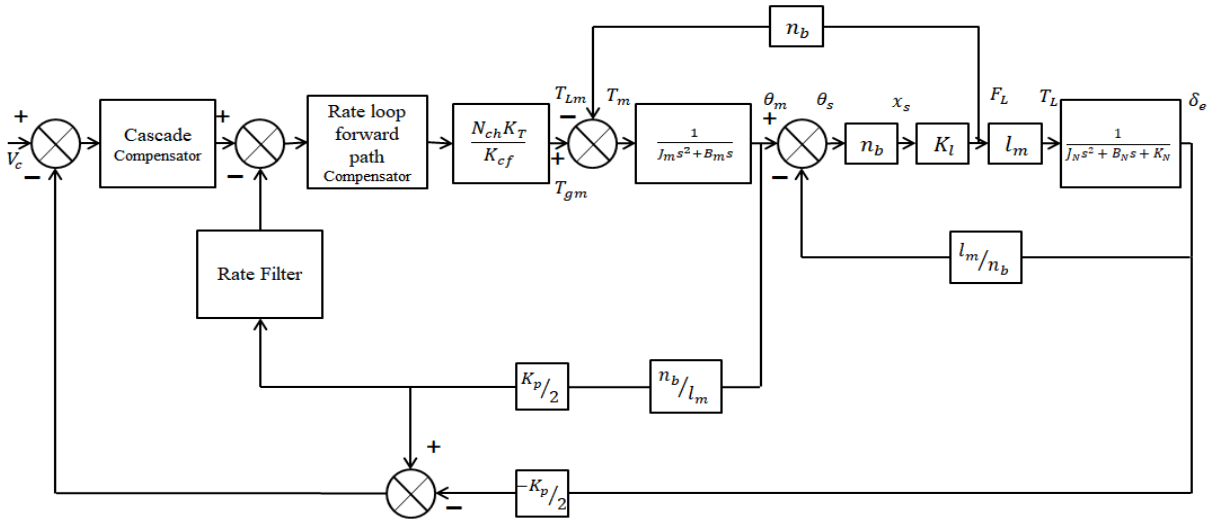

Figure 3.1: Linear Model of FNC System

The tuned parameter values for launch vehicle actuation system are given in Table 3.2.

Table 3.2: Parameter values for launch vehicle actuation system

Symbol	**Description**	**Value**
B_N	Viscous damping of engine gimbal	4000 Nm/rad/sec
B_m	Viscous damping of torque motor	0.004 Nm/rad/sec
J_N	Engine moment of inertia	60 kg-m^2
J_m	Moment of inertia of torque motor rotating assembly	1000 * 10^{-6} kg-m^2
K_b	Back emf constant	0.4
K_{cf}	Feedback gain of current loop	10/12.5 V/A
K_l	Equivalent stiffness of actuator mounting structure including all mechanical elements in series with actuator	0.6 * 10^7 N/m
K_N	Flex seal stiffness	1600 Nm/deg
K_p	Position sensor scale factor	286.47 V/rad
K_T	Torque sensitivity of motor	0.4 Nm/A
l_m	Actuator lever arm length	0.4 m
n_b	Ball screw gear ratio	6e-3/2/pi m/rad
N_{ch}	Number of operating channels of torque motor	4

3.3 Nonlinear FNC System

The nonlinearities in the FNC system are modeled as follows:

3.3.1 Current Loop Modeling

The FNC system uses a brushless DC torque motor. A ball screw mechanism converts the rotary motion of the motor to linear displacement, which will actuate the engine in the required plane. Hall sensor based six-pulse commutation and PWM based power amplifier are used in the BLDC motor. A high gain current loop is provided in the motor to nullify the effect of power supply variation and other motor parameter variation. The current loop has two operating regions.

The power amplifier stays in linear zone if,

$$|Z_m * i_m + K_b * \omega_m| < V_s \tag{3.20}$$

where,

$$\begin{aligned} Z_m &= \sqrt{(R_m)^2 + (X_m)^2} \\ X_m &= \omega_m * L_m \end{aligned} \tag{3.21}$$

where, R_m - DC torque motor coil resistance per coil

Z_m - Engine viscous damping coefficient

X_m - DC torque motor coil reactance per coil

L_m - DC torque motor coil inductance per coil

K_b - Motor back emf constant

ω_m - Motor angular velocity

V_s - Voltage applied across the coil

For the linear range of power amplifier, as the current loop has large bandwidth, the torque motor coil current is given by,

$$i_m = V_i * K_A \tag{3.22}$$

where, V_i - Power amplifier input voltage

K_A - Net power amplifier gain

The power amplifier becomes saturated when the condition mentioned above is violated, thereby opening the current loop. Under this condition the coil current can be obtained as,

$$i_m = \frac{V_s * sign(V_i) - K_b * \omega_m}{Z_m} \tag{3.23}$$

Total coil current is given by,

$$i = N_{ch} * i_m \tag{3.24}$$

3.3.2 Friction Modeling

The rotational motion is converted to linear motion using the ball screw, which causes friction in the motor. Stiction and coulomb friction are the two types of friction. When the rotor has a non-zero angular velocity, coulomb friction is continuous, and it applies a sustaining torque opposite to the direction of rotation, as given by [6].

$$T_c = F_c.sign(\omega_m) \tag{3.25}$$

Only when the effective driving torque on the rotor (Tdr) is greater than the stiction torque can the rotor escape from the stiction zone. The effective driving torque (Tdr) is defined as the gross torque developed within the motor minus the torque loss due to rotor damping and load dynamics. This is the net driving torque available to accelerate the motor rotating moment of inertia.

During running time, the friction is simulated in such a way that it should not act as a driving force causing sign reversal of the rotor velocity. This is achieved by checking the motor velocity at each simulation sampling interval with and without normal coulomb friction, using the previous velocity as initial condition. If both velocities ie., with and without normal coulomb friction have the same sign, then the assumption of coulomb friction in the normal sense is correct. However, if the signs are opposite, the sign reversal is caused by the coulomb friction and hence the motor velocity is forced to zero keeping under stiction domain. The actuator enters the stiction zone if,

$$(|T_{dr}| < F_c)\, and\, (\omega_{m1} * \omega_{m2} < 0) \tag{3.26}$$

The motor dynamic equations with and without frictions are as follows :

$$\dot{\omega}_{m1} = \frac{T_{dr} - T_c}{J_m} \tag{3.27}$$

$$\dot{\omega}_{m2} = \frac{T_{dr}}{J_m} \tag{3.28}$$

During stiction zone, $\omega_m = 0$ and during friction zone, $\omega_m = \omega_{m1}$

where, ω_{m1} - Motor velocity with coulomb friction

ω_{m2} - Motor velocity without coulomb friction

T_{dr} - Effective driving torque

T_s - Torque due to stiction

3.3.3 Stroke Limit Logic

Mechanical stroke of actuator is limited to Ls, when the output of the actuator exceeds this limit; it is limited to the mechanical stroke. As motor deflection is available as a state, the mechanical stroke limit is converted to equivalent motor deflection and the same is limited to the corresponding value. If,

$$|\theta_m| > \theta_{lim} \tag{3.29}$$

$$\theta_m = \theta_{lim} * sign(\theta_m) \tag{3.30}$$

where the equivalent actuator rotation deflection is given by,

$$\theta_{lim} = L_s/n_b \tag{3.31}$$

The implementation of stroke limit as mentioned above has some limitations. The logic is based only on the mechanical movement, but actually it is a function of force/torque applied also and velocity should be brought to zero during stroke limit. So, a new logic is designed and it can be used where stroke limit application and dynamics are very critical. Therefore, the mechanical stroke of actuator is limited when the output of actuator exceeds this limit in eqn. 3.22.

$$|X_{A1}| > \theta_{lim} \,\&\, (\omega_m * \theta_m) \geq 0 \tag{3.32}$$

where,

$$X_{A1} = \theta_{lim} * n_b \tag{3.33}$$

If eqn. is satisfied, the system is in stroke limit zone and,

$$\omega_m = 0 \,\&\, |\theta_m| = L_s/n_b \tag{3.34}$$

Once the system is in the stroke limit zone, it will come out from the stroke limit zone if the following condition satisfies.

$$\omega_m == 0 \,\&\, (T_{dr} * \theta_m) < 0 \tag{3.35}$$

where, θ_m - Motor angular position

θ_{lim} - Equivalent actuator deflection

L_s - Stroke length of actuator

3.3.4 Block Diagram of Nonlinear FNC System

The block diagram of the compensated non-linear FNC system is given in Fig. 3.2. This model is simulated in MATLAB/SIMULINK and the results are analysed to see if the required specifications have been met.

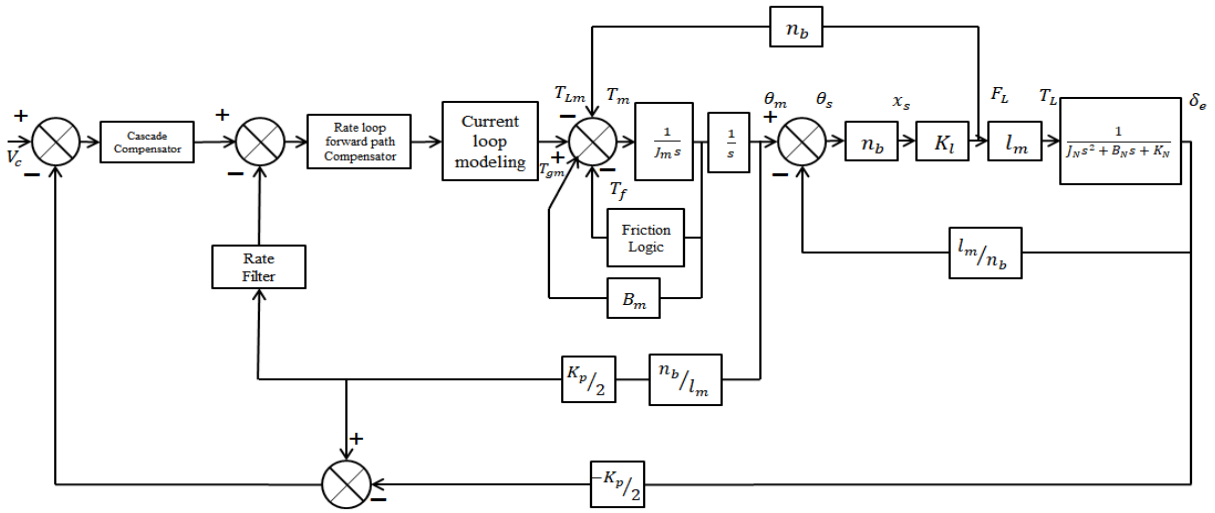

Figure 3.2: Nonlinear Model of FNC System

3.4 Concluding Remarks

This section dealt with the modeling of linear and nonlinear FNC system. The simulation results of the models are included in chapter 5. The next section is about the fault diagnosis methodology and the dataset generation.

Chapter 4

FAULT SIMULATION AND CLASSIFICATION

4.1 Dataset Generation

The parameter used for feature extraction is the motor current (i_m). In the EMA system, the motor current generally contains the fault information and is easy to measure. But directly from the motor signal, identification of the fault condition is not possible. Therefore, some features are to be extracted from them. For this, 1-D Wavelet Transform is used.

4.1.1 Wavelet Transform

WT is known for its effectiveness in feature extraction for fault diagnosis in machines. The information received from time-domain signals recorded in normal or fault conditions is often insufficient to detect defects in EMAs. DWT is used to convert time signals to time-frequency domain signals, allowing the varied properties of each current signal to be more clearly seen. ie, when the disturbance develops, big coefficients are displayed in various frequency bands. Depending on the prominent frequency components of the signals, the number of stages of decomposition is decided. The levels are adjusted so that the wavelet coefficients include only those parts of the signal that correspond well with the frequencies necessary for signal classification. The Daubechies basis of order four (db4) has been utilised in five levels of decomposition to generate distinct frequency bands of the signal in this process. To get effective discriminating results, all of these frequency component's properties are combined. The 1-D wavelet decom-

position tree is shown in Fig. 4.1 where five levels of decomposition of the current signal is done. When the wavelet transform is used to analyze a signal, it decomposes the signal into two components: detail and approximation coefficients as in eqn. 4.1.

$$S(n) = \sum_{i=1}^{i} D_i(n) + A_i(n) \tag{4.1}$$

where i is the level of decomposition. The coefficients obtained for five level decomposition are d_1, d_2, d_3, d_4, d_5 and a_5.

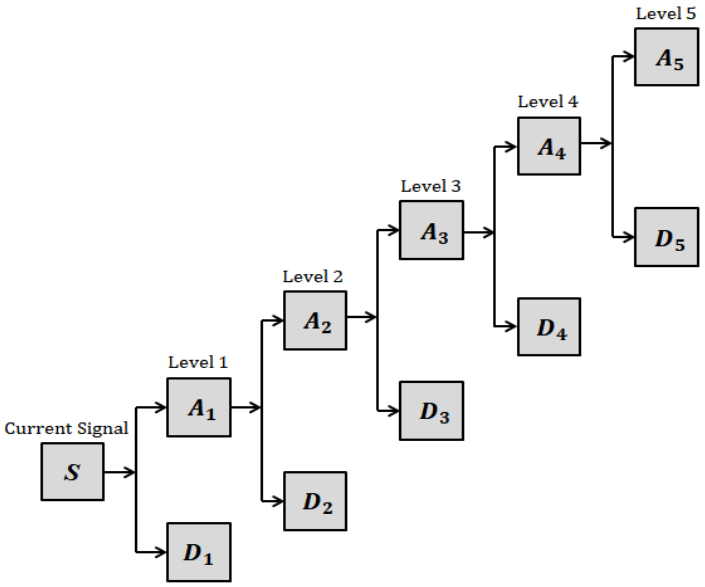

Figure 4.1: Current signal decomposition using 1-D WT

1-D WT is carried out using the Wavelet Analyzer Toolbox of MATLAB 2020b to decompose the motor current signal. The current signal decomposition is shown in Fig. 4.2.

4.1.2 Feature Extraction

Feature extraction is done by using the detail coefficients. For approximation coefficient, the signal 's' is convolved with a LPF, while for detail coefficient, it is convolved with a HPF. The lowpass wavelet coefficients are the approximation or scaling, coefficients, while the highpass wavelet coefficients are the details.

(i) **Maximum**

Maximum value of the detail coefficients d_1, d_2, d_3, d_4 and d_5. From each coefficient, one maximum value is obtained. From one signal decomposition, five features can be derived.

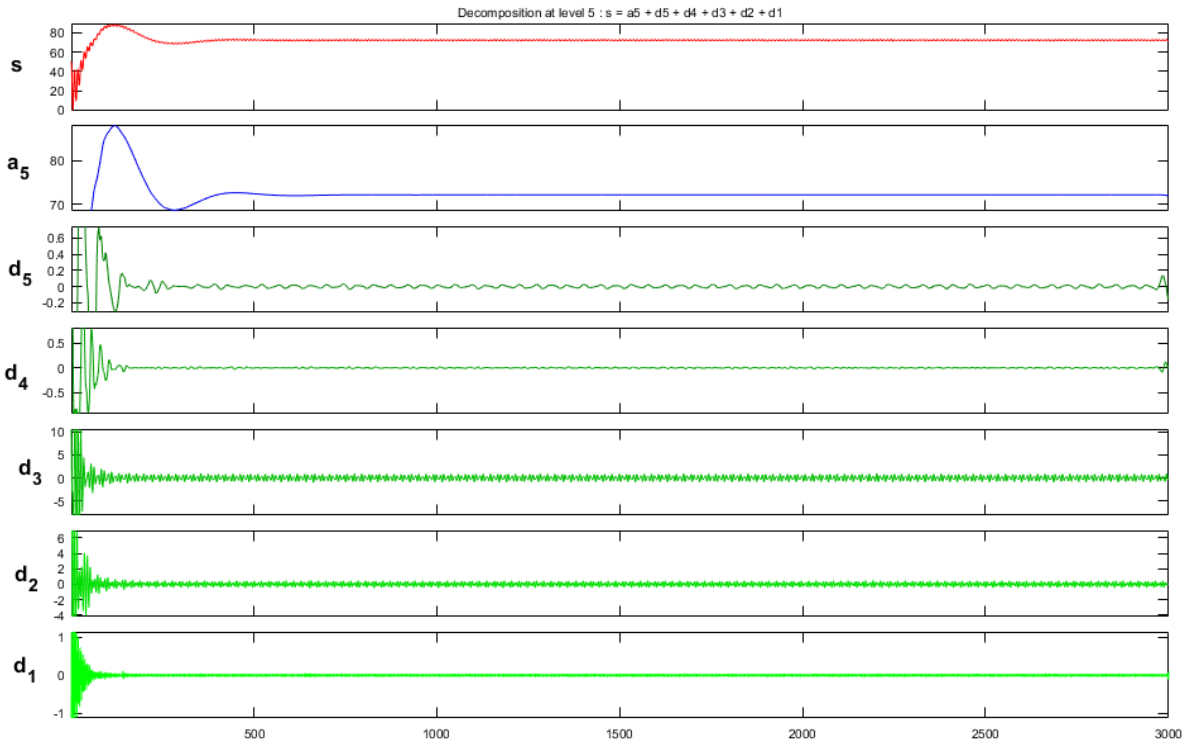

Figure 4.2: Signal decomposition using WT

(ii) **Minimum**

Minimum value of the detail coefficients d_1, d_2, d_3, d_4 and d_5. Five features can be derived from the detail coefficients in the 5 level decomposition of current signal.

(iii) **RMS**

Determined by squaring each value, determining the arithmetic mean of all those squared values, and taking the square root of the result [24].

$$RMS = \sqrt{\frac{1}{N}\sum_{i=1}^{N} D_i(n)} \tag{4.2}$$

where N is the count of sampling points and D_i is the amplitude

(iv) **Standard Deviation**

The standard deviation is a metric for determining how much a group of data varies or disperses. It is generally the square root of variance.

$$SD = \sqrt{\frac{1}{N-1}\sum_{i=1}^{N} |x_i - \mu|^2} \tag{4.3}$$

where x_i is the signal value, μ the population mean and N the number of sampling points.

(v) **Entropy**

Shannon entropy is used as a feature for fault detection in EMA system [23], [30]. Whenever a fault condition happens in the system, the system characteristics changes and shannon entropy of the system also changes. Shannon entropy has the energy information about the signal. Thus it can be used as a good feature for fault analysis.

$$EN = \sum_{i=1}^{N} D_i^2 \, log(D_i)^2 \tag{4.4}$$

where D_i is the coefficient of details or approximation of signal after WT.

A variety of tests are carried out using several forms of wavelet, with the most efficient wavelet being chosen for decomposition. The Daubechies wavelet is recognised for identifying frequency changes. As a result, Daubechies (Db4) wavelet is used for wavelet transform of the motor current signal. 25 features are obtained from the detail coefficients, which is the input to wavelet neural network.

4.2 Fault Simulations

The common faults occurring in the actuation system is simulated to generate the dataset. Five system conditions to be classified are:

(i) **Healthy**

First class of the WNN classifier. The FNC system remains in its state of healthy for a 2%-5% change in parameters. Data of the healthy system is simulated by varying the parameters by that margin and simulating the system with those values.

(ii) **Fault 1 (Motor Fault)**

Motor Faults belong to class 2 in the WNN classifier. For generating a motor fault, the number of operating channels N_{ch} is replaced by 3.

(iii) **Fault 2 (Sensor Fault)**

A 25% change in the scale factor is introduced to generate a scaling factor fault. Sensor faults belong to class 3.

(iv) **Fault 3 (Compensator Fault)**

Another common fault that occur in FNC actuation system is the compensator fault, where the output of the compensator is zero.

(v) **Fault 4 (External Disturbance)**

For initial simulations, the external load disturbance is zero. For simulating a fault condition, external disturbance is added to the system. This belongs to class 5.

4.3 WNN Classifier

Initialization and network training define a major portion of the computing resource needs. Improper initialization technique selection can increase computational costs while training. Effective initializing method selection can lower the number of network training iterations. The selection of mother wavelet can have a considerable impact. A wavelet neural network that is tailored to solve a specific problem can be obtained by selecting the mother wavelet.

The feature vector of the fault signal is linked to the input neurons of the networks, as shown in Fig. 4.3 The hidden layer activation function is derived from mother wavelet [26]. The hidden neuron activation function is derived from mother wavelet. The Morlet wavelet is used as the mother wavelet in the work.

The Wavelet Neural Network (WNN) used in the work has three layers: an input layer, a hidden layer and an output layer. Each layer is having more than one node [24], [25].

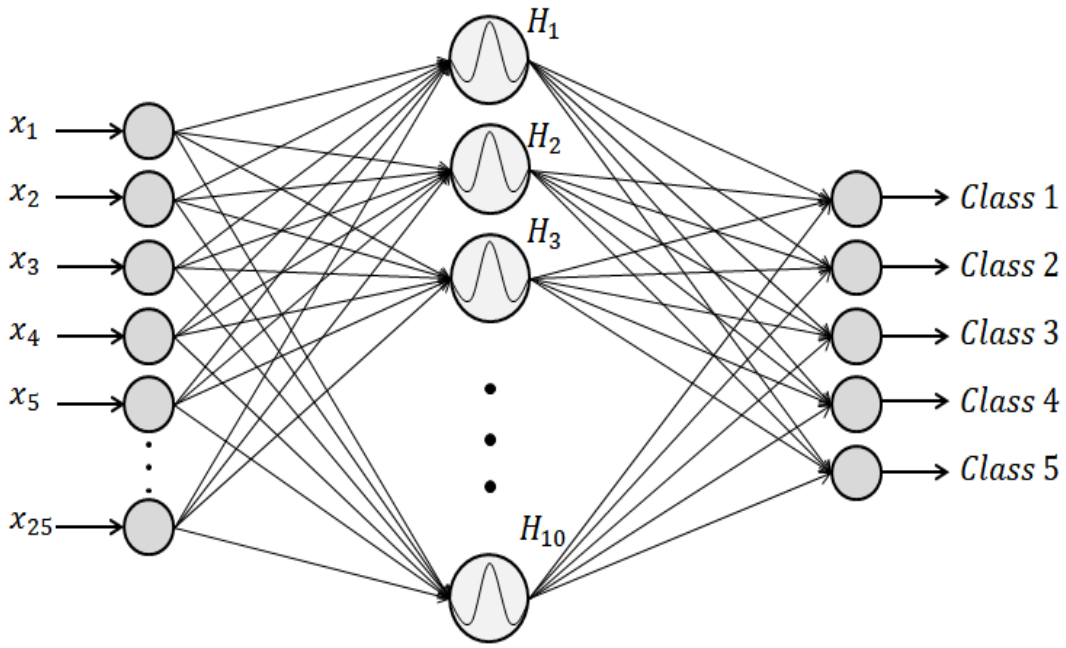

Figure 4.3: WNN Classifier

A 25×10×5 classifier used for classifying the FNC actuation system conditions is shown in Fig. 4.3. The feature vector X at the input layer contains twenty-five feature values.

$$X = [X_1\ X_2\ X_3\ ...\ X_{25}] \tag{4.5}$$

By empirical research outcomes, 10 nodes are created at the hidden layer. The weights between input and hidden nodes are represented by w_{ij}. The hidden node's input is computed by the eqn. 4.6.

$$net_j = \sum_{i=1}^{25} w_{ij}\, X_i \tag{4.6}$$

where $j = 1, 2, 3, ...10$. The hidden node's output is computed by the eqn. 4.7

$$H_j(net_j) = H\left(\frac{net_j - b_j}{a_j}\right) \tag{4.7}$$

Wavelet activation function is given by H_{ij}, with scaling factor a_j and translation factor b_j as wavelet parameters.

Since the WNN is used for EMA system fault diagnosis and for the categorization of fault data, it is classified as pattern recognition and does not require orthogonality consideration. As a result, the Morlet wavelet function is chosen as the activation function for the neural network since it is a cosine modulated Gaussian wavelet with a good time-frequency resolution [18]. The Morlet wavelet used as wavelet function is represented as,

$$H(t) = cos(1.75t)\, exp(-0.5t^2) \tag{4.8}$$

Five output nodes apply linear activation function to form the output vector Y specified in the output layer. The output vector Y is given by

$$Y = [Y_1\ Y_2\ Y_3\ ...\ Y_5] \tag{4.9}$$

The weights connecting output node and hidden node are represented by w_{jk}.

$$Y = \sum_{j=1}^{10} w_{jk}\, H_j(net_j) \tag{4.10}$$

By feeding information forward and error backward, mean square error performance function is intended to approach a minimum. The mean square error function is represented by,

$$Error = \frac{1}{n}\sum_{k=1}^{n}(Y_k - d_k)^2 \tag{4.11}$$

where d_k is the desired output at the k^{th} node The key parameters are repeatedly determined using the updated laws below [27], [24].

$$w_{ijnew} = -\eta_1 \frac{\delta Error}{\delta w_{ij}} + w_{ijold} \tag{4.12}$$

$$w_{jknew} = -\eta_2 \frac{\delta Error}{\delta w_{jk}} + w_{jkold} \tag{4.13}$$

$$a_{jnew} = -\eta_3 \frac{\delta Error}{\delta a_j} + a_{jold} \tag{4.14}$$

$$b_{jnew} = -\eta_4 \frac{\delta Error}{\delta b_j} + b_{jold} \tag{4.15}$$

d_k is the intended output of the output layer, and η_1, η_2, η_3, and η_4 are learning rates. The values set for learning rates are :

$$\eta_1 = 0.01 \tag{4.16}$$

$$\eta_2 = 0.01 \tag{4.17}$$

$$\eta_3 = 0.001 \tag{4.18}$$

$$\eta_4 = 0.001 \tag{4.19}$$

The training continues until the accuracy condition is satisfied or when reaching the maximum number of epochs. Fig. 4.4 shows the flowchart of WNN classifier training.

The dataset is generated by using the methodology of wavelet transform that contains 200 samples with 25 input features. The features considered were maximum, minimum, RMS, standard deviation and the shannon entropy. These were obtained from the detail coefficients of wavelet decomposition. The data were input to the 25×10×5 wavelet neural network classifier.

For training and testing procedures of WNN, data was split into two groups. 200 examples were evaluated in order to validate the suggested classifier. 140 random samples were used to train the networks and 60 of them were utilized to test the trained network.

After the network has been trained, test data is given to see the accuracy of network in classifying the fault. Following the training, 60 random samples are utilised for testing.

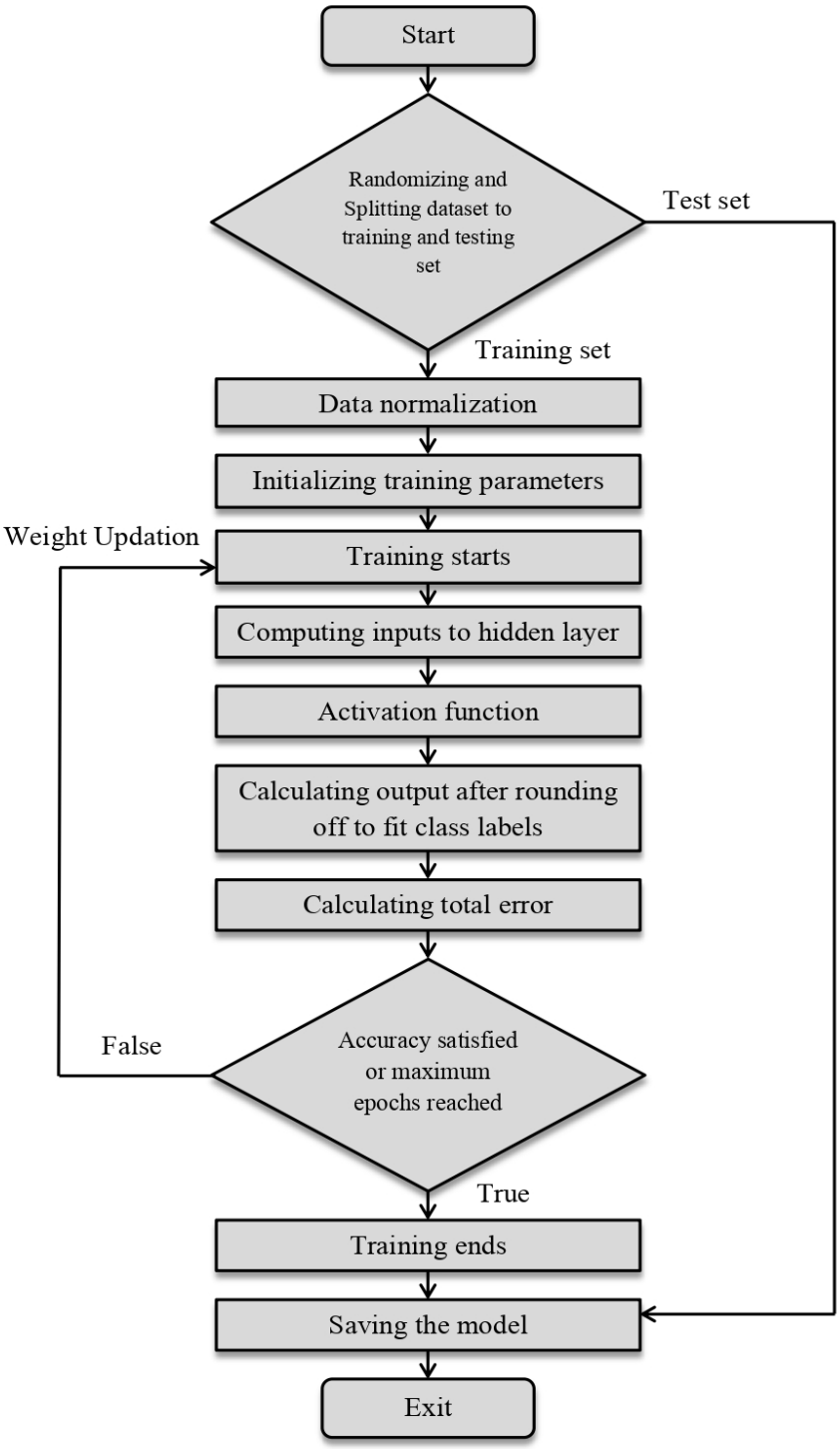

Figure 4.4: Flowchart of WNN classifier training

4.4 ANN Classifier

To compare the effectiveness of the WNN classifier, an ANN classifier was designed, shown in Fig. 4.5. The ANN has the same structure as the WNN. The activation function used for hidden neurons was Tan-Sigmoid with the same number of hidden neurons. Learning algorithm used is gradient descent.

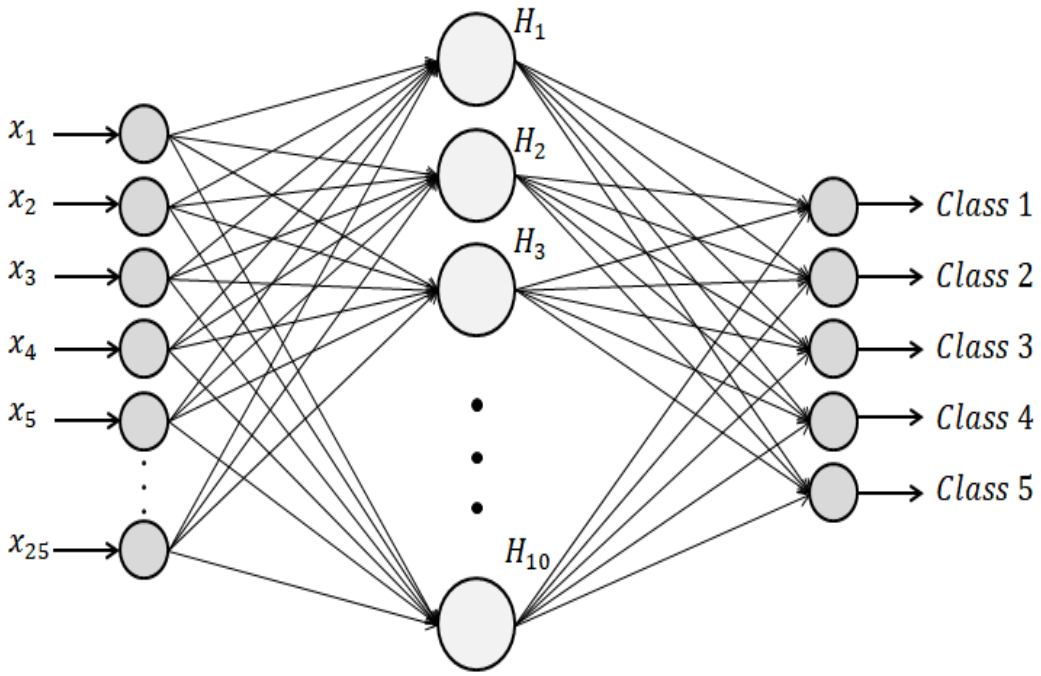

Figure 4.5: ANN Classifier

4.5 Concluding Remarks

In this chapter, the common possible faults in the FNC system was identified and was simulated. Feature extraction was done using WT. A WNN classifier was designed to classify the fault conditions and compare its effectiveness with the ANN. The simulation's findings and evaluations are presented in the next chapter.

Chapter 5

RESULTS AND DISCUSSION

5.1 Linear FNC System Response

The linear model of FNC system (Fig. 3.2) was modeled in MATLAB/Simulink and the step response obtained for the compensated linear model is as in Fig 5.1. It can be seen that the servo system is tracking the input command.

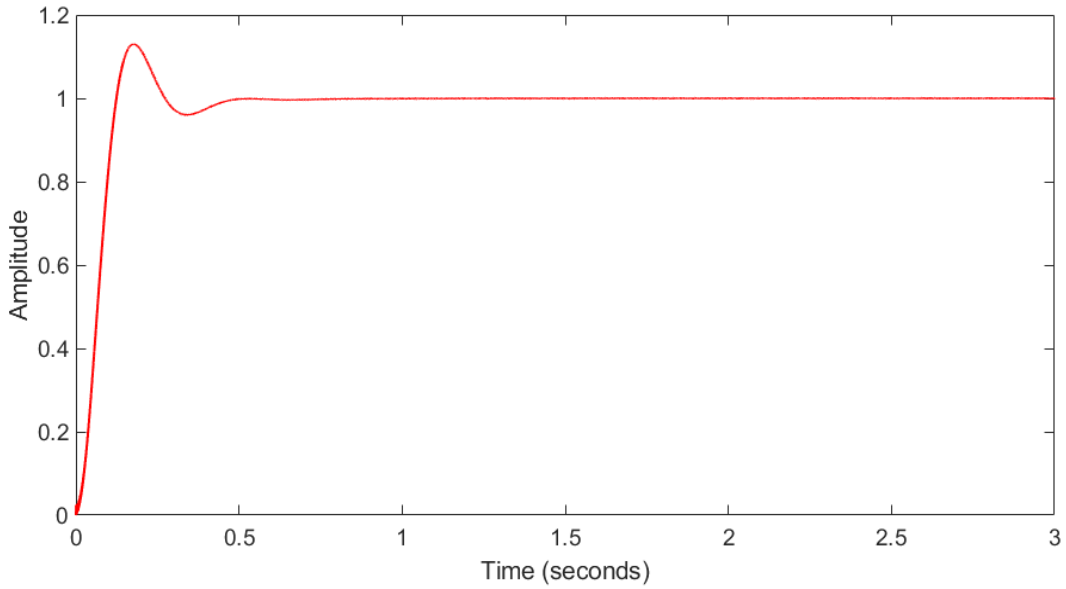

Figure 5.1: Step Response of Linear FNC System

Table 5.1: Time Domain Specifications

No.	Specification	Obtained Values
1	Settling time	$424ms$
2	Maximum peak overshoot	13%
3	Peak time	$167ms$
4	Rise time	$122ms$
5	Steady state error	0%

5.2 Nonlinear FNC System Response

The influence of nonlinearities is mostly seen in the system's response with sine input. At the maximum, the response appears to be somewhat distorted. Coulomb friction is thought to be the primary source of the motor's nonlinear behaviour [6]. Fig. 5.2 shows the sinusoidal response of the system with nonlinearities as mentioned in section 3.3, when the input frequency is 1rad/s.

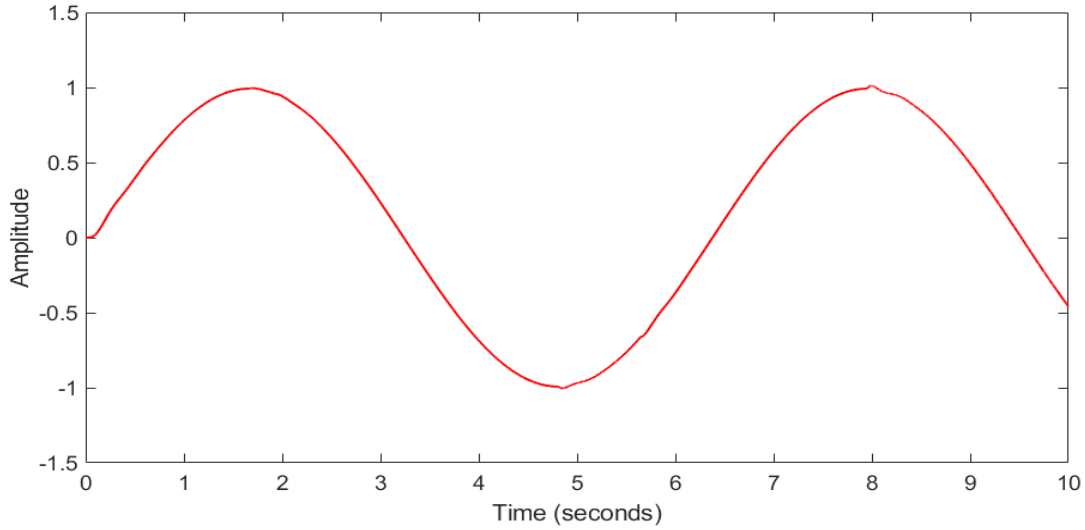

Figure 5.2: Sinusoidal Response of Nonlinear FNC System

5.3 Fault Classifier using WNN

Fig 5.3 shows the training confusion matrix that given 100% accuracy on training the data.

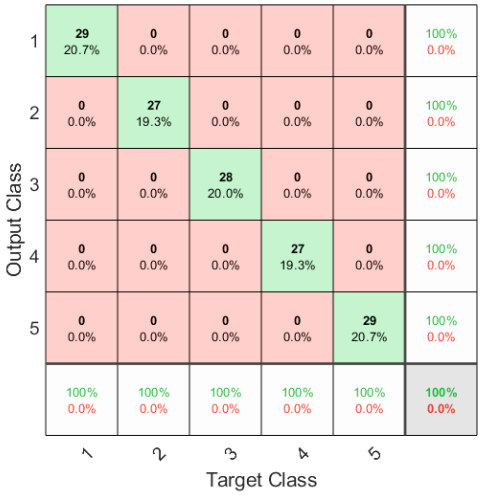

Figure 5.3: Training Confusion Matrix

Fig. 5.4 shows the confusion matrix acquired during the testing phase. It has a 96.7% accuracy rate. There was only two samples that was misclassified. This implies that the WNN architecture produces extremely precise results. As illustrated, there occurs a misclassification as a measure of classification uncertainty between classes 3 and 4 (Sensor and compensator fault).

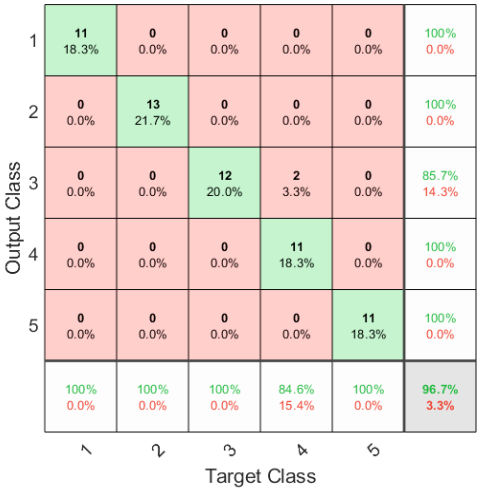

Figure 5.4: Testing Confusion Matrix

Fig. 5.5 depicts the convergence of the mean square error (MSE) with respect to epochs during training and testing of the network.

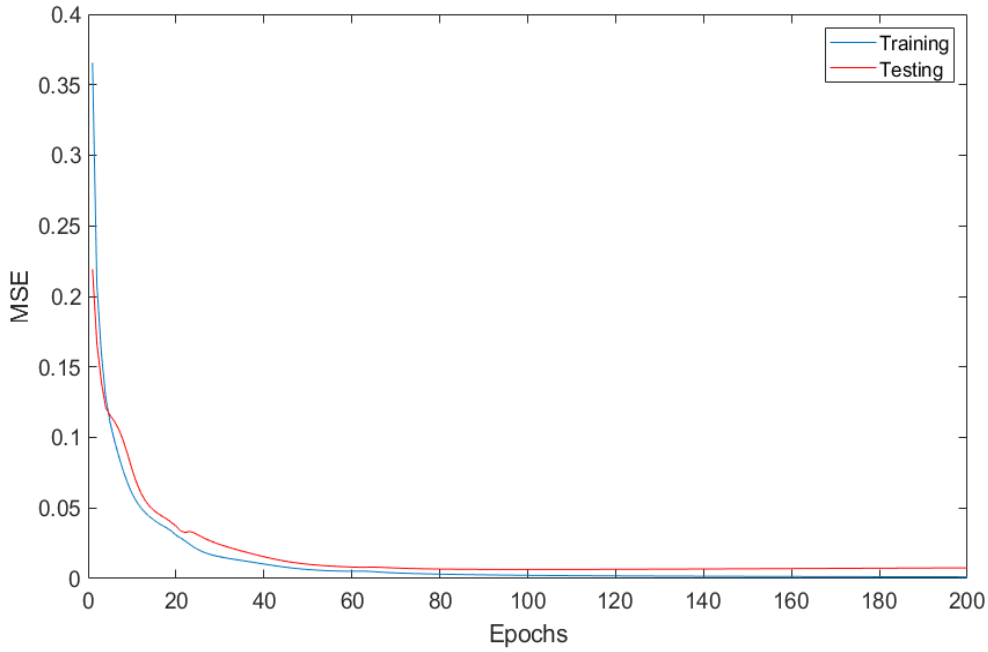

Figure 5.5: Mean Square Error

The WNN model's accuracy curves for the training and testing stages are displayed in Fig. 5.6.

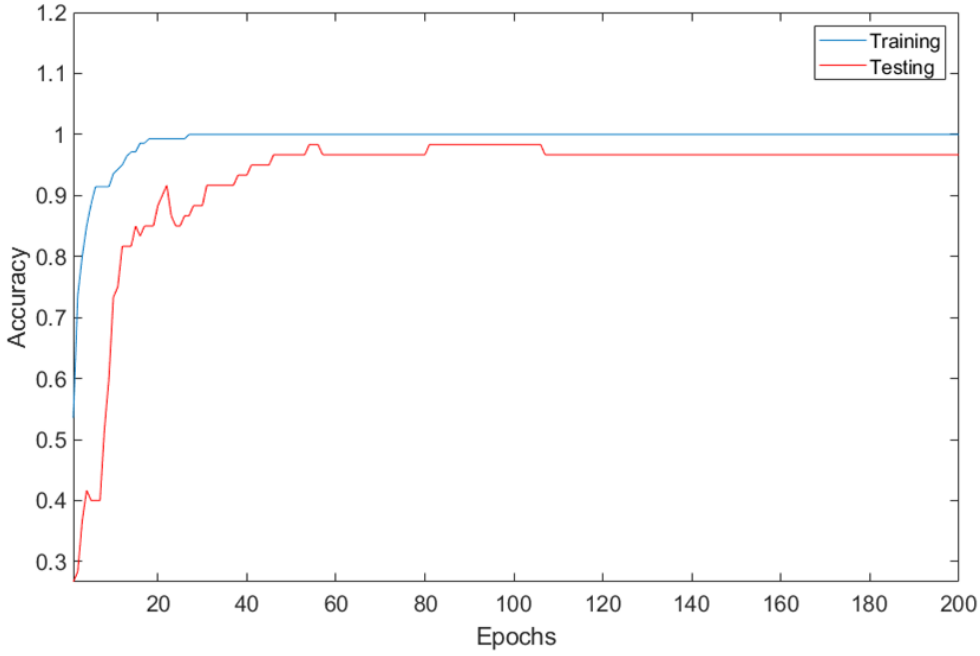

Figure 5.6: Training and Testing Accuracy

The Morlet wavelet's simplicity can be attributed to this signal processing method's ability to reduce undesired modulation effects. As a result, usage of this particular method has shown to be a useful technique for detecting faults in launch vehicle actuation systems.

In order to verify the accuracy of the wavelet neural network, this work uses the WNN for fault recognition of the test samples. The above results demonstrate that the WNN is designed to produce very accurate outcomes.

5.4 Comparison of WNN with ANN Classifier

The training accuracy obtained for fault classification is shown in Fig. 5.7. It can be observed that the accuracy is 80%, where class 3 (sensor fault) cannot be identified by the conventional ANN even after feature extraction is done. Utilizing WNN helps to address this drawback.

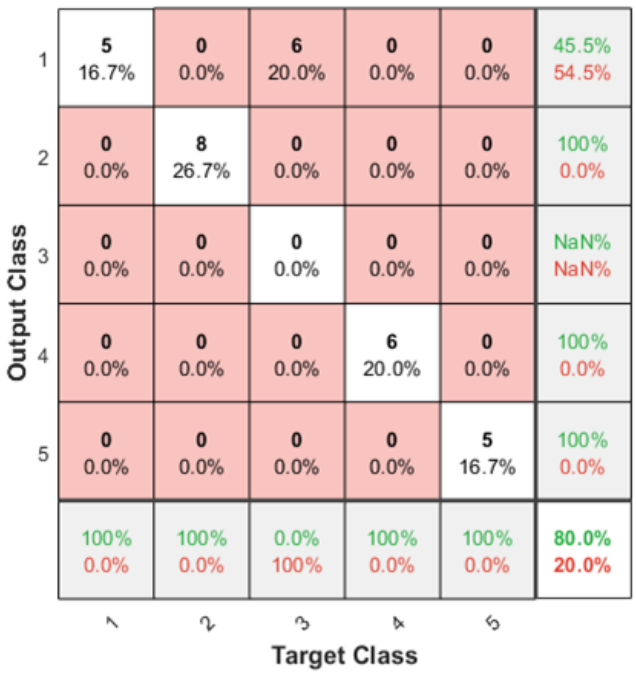

Figure 5.7: ANN Training Confusion Matrix

Chapter 6

CONCLUSION

The modeling, implementation and analysis of a flex nozzle control system of the launch vehicle actuation system is presented. The proposed scheme for fault diagnosis of launch vehicle actuation system is by using Morlet wavelet based Wavelet Neural Network (WNN). Wavelet Transform (WT) based feature extraction technique is adopted for this classification problem. The adaptive learning is utilized to optimize the gradient descent algorithm for training the neural network. The proposed classifier, which consists of five classes, was implemented and the system model was also simulated using MATLAB/SIMULINK. The WNN was found to have an accuracy of 96.7% in classifying the system conditions and is more effective than ANN in classification.

REFERENCES

[1] P. Biju, R. Sandeep, R. Aravind, P. Kumar, and U. Naik, “Optimum Design of a Fault Tolerant Linear Electromechanical Actuator for the Lower Stage Thrust Vector Control of a Satellite Launch Vehicle”, in *European Space Mechanisms Tribology Symposium-ESMATS 2011 Constance*, 2011.

[2] D. Swain, S. K. Biswal, B. P. Thomas, S. S. Babu, and J. Philip, “Performance characterization of a Flexible Nozzle System (FNS) of a Large Solid Rocket Booster Using 3-D DIC,” *Experimental Techniques*, vol. 43, no. 4, pp. 429–443, 2019.

[3] A. E Kumar, K. S Sastry, K. Manideep, M. Priyanka, “Dynamic Analysis of Flex Seal of Solid Rocket Motor Nozzle,” *Materials Today: Proceedings*, vol. 4, no.2, pp.1590-1597, 2017

[4] G. B Kumar, B. Sebastian and B.M Varghese,“Servo Design of Electromechanical ActuatorBased System for Launch Vehicle Applications,”*International Journal of Advanced Research in Electrical, Electronics and Instrumentation Energy*, vol. 2, pp. 1963-1969

[5] S. R. Anas, H. Jaison, A. Gopinath, M. N. Namboothiripad and M. P. Nandakumar, “Modeling and simulation analysis of a redundant electromechanical actuator based position servo system,” *2011 International Conference on Computer, Communication and Electrical Technology (ICCCET)*, pp. 358-363, 2011

[6] A. M. Kuriakose, P. C. Kurian and L. P. P S., "Optimized Servo Design of SS2 Flex Nozzle Control System for Small Satellite Launch Vehicle,” 2020 International Conference on Power, *Instrumentation, Control and Computing (PICC)*, pp. 1-6, Dec 2020

[7] S. Krishnamani and T. Mohanraj, "Fault Tolerant Servo Actuation System using MRAC for Launch Vehicle Electromechanical Actuator,” *Indian Journal of Science and Technology*, vol. 9, no.45, pp. 1-10, Dec. 2016

[8] A. Sebastian, P. Thomas, and S. Alex, “Servo design and analysis of thrust vector control of launch vehicle,” in *2017 Innovations in Power and Advanced Computing Technologies (i-PACT)*, pp. 1–5, IEEE, 2017.

[9] P. Suchitra, P. C. Kurian, and S. R. Jones, "Optimal controller based servo system design for the thrust vector control of liquid propellant engine of three stage launch vehicle," in *2014 Annual International Conference on Emerging Research Areas: Magnetics, Machines and Drives (AICERA/iCMMD)*, pp. 1–6, IEEE, 2014.

[10] NewSpace India Limited (NSIL), "Small satellite launch vehicle technical brochure," Sept. 24 2019. ISRO.

[11] A. E. Kumar, K. S. Sastry, K. Manideep, and M. Priyanka, "Dynamic analysis of flex seal of solid rocket motor nozzle," *Materials Today: Proceedings*, vol. 4, no. 2, pp. 1590–1597, 2017

[12] E. Balaban et al., "A diagnostic approach for electro-mechanical actuators in aerospace systems," in *2009 IEEE Aerospace Conference*, pp. 1-13, Feb. 2009

[13] X. X. Li, Q. J. Zhang and H. J Xiao, "The design of brushless DC motor servo system based on wavelet ANN," *Proceedings of 2004 International Conference on Machine Learning and Cybernetics (IEEE Cat. No.04EX826)*, pp. 929-933, vol.2, 2005

[14] J. Yang, Z. Yang and X. Sun, "Modeling and fault analysis of brushless DC motor for electromechanical actuator," *2016 IEEE International Conference on Aircraft Utility Systems (AUS)*, pp. 852-856, 2016

[15] H. Liu, D. Li, C. Lu and D. Liu, "Fault diagnosis for a hydraulic servo system using wavelet packet and neural network," *2016 12th World Congress on Intelligent Control and Automation (WCICA)*, pp. 1981-1985, 2016

[16] F. Charfi, F. Sellami and K. Al-Haddad, "Fault Diagnostic in Power System Using Wavelet Transforms and Neural Networks," *2006 IEEE International Symposium on Industrial Electronics*, pp. 1143-1148, 2006

[17] M. Jayakumar and B. B. Das, "Fault Detection, Isolation and Reconfiguration in Presence of Incipient Sensor Faults in an Electromechanical Flight Control Actuation System," *2006 IEEE International Conference on Industrial Technology*, pp. 92-97, 2006

[18] G. Zhou, G. Liu and Y. Luo, "Asynchronous Motor Fault Diagnosis Based on Wavelet Neural Network," *2009 International Conference on Information Engineering and Computer Science*, pp. 1-4, 2009

[19] S. M. K. Zaman, H. U. M. Marma and X. Liang, "Broken Rotor Bar Fault Diagnosis for Induction Motors Using Power Spectral Density and Complex Continuous Wavelet Transform Methods,"

2019 IEEE Canadian Conference of Electrical and Computer Engineering (CCECE), pp. 1-4, 2019

[20] A. B. Stepanov, "Construction of activation functions for wavelet neural networks," *2017 XX IEEE International Conference on Soft Computing and Measurements (SCM)*, pp. 397-399, 2017

[21] H. Li, "Bearing fault diagnosis based on time scale spectrum of continuous wavelet transform," *2011 Eighth International Conference on Fuzzy Systems and Knowledge Discovery (FSKD)*, pp. 1934-1937, 2011

[22] Q. Y Xu, X. Y Meng, X, J Han and S. Meng, "Gas turbine fault diagnosis based on wavelet neural network," *2007 International Conference on Wavelet Analysis and Pattern Recognition*, pp. 738-741, 2007

[23] A. N. Kannan and A. Rathinam, "High Impedance Fault Classification Using Wavelet Transform and Artificial Neural Network," *2012 Fourth International Conference on Computational Intelligence and Communication Networks*, pp. 831-837, 2012

[24] Y. Jin, C. Shan, Y. Wu, Y. Xia, Y. Zhang and L. Zeng, "Fault Diagnosis of Hydraulic Seal Wear and Internal Leakage Using Wavelets and Wavelet Neural Network," *IEEE Transactions on Instrumentation and Measurement*, vol. 68, no.4, pp. 1026-1034, Apr. 2019

[25] X. Yin, Z. Zhang, A.M Liu and Q.L Li, "Pattern recognition of super-alloy friction welding joint defect by wavelet packet and wavelet neural network," *2007 International Conference on Wavelet Analysis and Pattern Recognition*, pp. 761-76, 2007

[26] S. Qiang and Y. Li, "Motor Inverter Fault Diagnosis Using Wavelets Neural Networks," *2013 IEEE International Conference on Systems, Man, and Cybernetics*, pp. 3168-3173, 2013

[27] Zhi-Yong Luo and Zhong-Ke Shi, "Wavelet neural network method for fault diagnosis of push-pull circuits," *2005 International Conference on Machine Learning and Cybernetics*, pp. 3327-3332 Vol. 6, 2005

[28] A. Y. Goharrizi and N. Sepehri, "A wavelet-based approach to internal seal damage diagnosis in hydraulic actuators," *IEEE Trans. Ind. Electron., vol. 57, no. 5, pp. 1755–1763*, May 2010

[29] A. Sadeghian, Z. M. Ye, and B. Wu, "Online detection of broken rotor bars in induction motors by wavelet packet decomposition and artificial neural networks," *IEEE Trans. Instrum. Meas.*, vol. 58, no. 7, pp. 2253–2262, Jul. 2009.

[30] S. E Safty, A. E Zonkoly. "Applying wavelet entropy principle in fault classification," *Electric Power Systems Research* , pp. 604-608, 2009

List of Publications

[1] A. Vijayan, B. Sebastian, A. Ravindranath, "Fault Diagnosis of a Launch Vehicle Actuation System using Wavelet Neural Network," *International Conference on Computing, Electronics Communications Engineering (iCCECE '22)*, 2022. (Under Review)